

Received November 12, 2020, accepted November 25, 2020, date of publication December 2, 2020, date of current version December 16, 2020.

Digital Object Identifier 10.1109/ACCESS.2020.3041370

Study on the Control Method and Optimization Experiment of Prostate Soft Tissue Puncture

YONGDE ZHANG¹, BING LI¹, AND LIPENG YUAN²

¹Robotics and Its Engineering Research Center, School of Mechanical Power Engineering, Harbin University of Science and Technology, Harbin 150080, China

²School of Mechatronics Engineering, Harbin Institute of Technology, Harbin 150000, China

Corresponding author: Yongde Zhang (zhangyd@hrbust.edu.cn)

This research was partly supported by the National Natural Science Foundation of China (NSFC), project no. 51675142. Part of the fund was allocated by the key project ZD2018013 at the Natural Science Foundation of Heilongjiang Province, China.

ABSTRACT In the treatment of prostate cancer patients, surgery of radioactive seed implantation with the puncture robots is an effective treatment method. However, when the puncture needle enters the lesion tissue, there are complicated forces between the needle body and the soft tissue, which leads to the drift of the prostate and the deflection of the puncture needle, thereby affecting the puncture accuracy. In order to improve the positioning accuracy and ensure the best treatment effect, a sine rotation continuous puncture control method was proposed in this paper. First, by analyzing the interaction between the puncture needle and the soft tissue, the force balance equation and the deflection equation were established, according to the equations, it could be known that puncture friction is the main factor affecting the deflection of the puncture needle. Second, combined with the influence of puncture friction and the research on the theory of rotation puncture, the sine rotation puncture method was compared with the direct puncture method and the existing rotation puncture method; Observed with a 4D Color Doppler Ultrasound to verify the feasibility of the rotating puncture theory and the effectiveness of the sine rotation puncture method. Third, through the establishment of Euler Beam model, rotation angle analysis and puncture velocity test analysis, the influence of dynamic parameters of this method on the puncture accuracy was discussed, the optimization range of each factor was obtained; The experiment was designed by the quadratic regression orthogonal combination theory, the experiment process was observed and recorded by a 3D X-ray scanner, the regression equations were established between experiment factors and experiment indicators with the Design-Expert, and the best parameter combinations were acquired through optimization. Last, comparison tests and verification test were carried out to verify the rationality and reliability of the optimized sine rotation puncture control method.


INDEX TERMS Control, deflection angle, optimization experiment, prostate soft tissue, puncture accuracy, puncture needle, sine rotation puncture theory, regression equation.

I. INTRODUCTION

Among the diseases of the urinary system, prostate cancer is one of the most common malignant tumors in male crowd, and its incidence is increasing year by year [1], [2]. According to statistics, prostate cancer is second only to lung cancer among male patients [3]–[6], and the incidence in China and other Asian countries are also increasing and tending to be younger [7]–[13]. At present, the treatment of prostate cancer mainly uses the minimally invasive surgical method of radioactive seed implantation, and the traditional surgery is mainly performed by doctors manually or using robots to complete related operations [14]. However, due to the

uncertainty of the doctor's operation, it is not only difficult to guarantee the positioning accuracy, but also causes severe trauma to the soft tissues, thereby affecting the treatment effect [15], [16].

With the continuous development of modern robotics technology, since the end of last century, robotics had been applied to clinical surgery for the first time, and a large number of scholars had been devoted to the research of medical robot [17]–[19]. Among them, minimally invasive surgical robot has the most promising development in the field of medical robots in the future. It not only has high positioning accuracy, good stability of motion, flexible and continuous working ability, but also it causes little trauma to patients and conducive to postoperative recovery [20]. So, regarding the operation of urological puncture surgery,

The associate editor coordinating the review of this manuscript and approving it for publication was Chao-Yang Chen .

Da Vinci Xi, a minimally invasive surgical robot developed by the American ISRG company in 2014 is mainly used in most countries and regions [21]. It has four operating arms attached to a rotating bracket that can move towards any part of the patient's body, and an endoscope that can be attached to any operating arm. In addition, it has a small robotic arm that can reduce collisions between them and offers a wider range of motion, mainly used to assist doctors in precise and complex minimally invasive surgery [14].

Although the use of minimally invasive surgical robots can accurately implant radioactive particles such as I235 and I125 at the planned target, and it can effectively reduce the number of repeated punctures and seed implants, improve the uniform distribution of dosimetry in the target region, and reduce postoperative complications [22]. However, if a direct puncture method is used during surgery, the puncture needle will easily deflect in the soft tissue [23], [24]. Therefore, many related scholars have conducted a lot of research in the field of prostate cancer puncture control technology.

Minhas *et al.* [25] studied a puncture control method of the needle rotation duty ratio, which could effectively reduce the deflection of the puncture path by precisely controlling the ratio of needle rotation and needle puncture time. Majewicz *et al.* [26] further studied the needle body alternate rotation puncture control method to improve the positioning accuracy of the puncture needle. Mahvash *et al.* [27] conducted a bovine heart puncture test and believed that when the needle punctures the epidermis of soft tissue, increasing the puncture velocity can reduce the propagation and deformation of the needle tip torn soft tissue, and reduce needle body deviation and soft tissue damage; Yinshan *et al.* [28], [29] proposed a fuzzy control puncture method based on force/position feedback; When the puncture needle enters the pig liver tissue, the robot stops the needle until the soft tissue returns to a relaxed state, and then performs puncture at a half velocity, thereby improving its puncture accuracy. Zhang *et al.* [30] designed a high accuracy puncture strategy based on vibration and rotation to reduce the friction of the soft tissue of the robot during the puncture process, and improve the deformation of the soft tissue of the prostate during the puncture process.

In addition, Reed *et al.* [31] designed a robot-assisted needle steering system that uses three integrated controllers: a motion planner concerned with guiding the needle around obstacles to a target for a desired plane, a planar controller that maintains the needle in the desired plane, and a torsion compensator that controls the needle tip orientation about the axis of the needle shaft; The system can effectively improve puncture accuracy. Li *et al.* [32] proposed a real-time model updating method of needle steering in non-uniform tissue for reducing the puncture error of soft tissue; This method designs a puncture needle integrated with FBG sensor and reconstructs its tip according to the fourth-order polynomial method; Meanwhile, it also controls the puncture trajectory according to the bicycle model and combines with MRI for navigation.

In summary, they mainly used intermittent control to change the motion state of the puncture needle in the soft tissue, thereby reducing the deflection of the puncture needle and reducing the damage to the soft tissue. However, during the actual operation of the above puncture method, it is difficult for the doctor to control the nodes that need to stop or change the motion state, or the larger puncture error may be caused due to operation error.

In order to reduce the deflection problem caused by the robot during the puncture of prostate soft tissue, improve the puncture accuracy, and ensure the treatment effect and reduce the difficulty of the doctor's operation; Therefore, it was necessary to further research and optimize the control method of the puncture of the prostate soft tissue. So, this paper was organized as follows: In Section 2, analyzed the interaction between the puncture needle and the soft tissue, understood the main reason for the deflection of the puncture needle when puncturing the soft tissue, and built a test platform to ensure subsequent theoretical research. In Section 3, The existing puncture control theory and method were introduced and analyzed in detail, and a sine rotation continuous puncture control method was proposed in this paper, which was proved to be feasible and effective by performance test. In Section 4, The control parameters that affect puncture deflection were deeply analyzed and studied, and the optimal range of control parameters was obtained. In Section 5, combined with the optimization ranges and indices of the control parameters, the optimal control parameters were obtained through experimental research. In Section 6, used performance comparative verification tests, the rationality of the control method of the sine rotation puncture soft tissue and the reliability of the optimal parameters were verified. The paper was concluded in the last section.

II. PRINCIPLE ANALYSIS AND TEST PLATFORM

When doctors use robots to implant radioactive seed through perineum to treat prostate cancer, the interaction between puncture needle and soft tissue can cause problems that drift and deformation of soft tissue and needle body deflection, so that radioactive particles cannot be accurately implanted into the target point, which will affect treatment effect. In order to improve positioning accuracy of prostate radioactive seed implantation, it was necessary to analyze the process of soft tissue puncture by needle.

In addition, in order to ensure the follow-up theoretical research, a test platform was built according to the design requirements of the prostate soft tissue puncture robot.

A. PUNCTURE PROCESS ANALYSIS

1) FORCE ANALYSIS

In the process of prostatic soft tissue puncture, the body and tip of the puncture needle (It belongs to medical surgical semi-flexible seed implantation needle) will be subjected to the force of the soft tissue, which is the main reasons for the deflection of the puncture needle in the soft tissue of

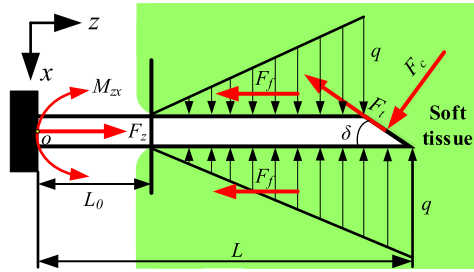


FIGURE 1. The force analysis diagram of acupuncture soft tissue.

the prostate and gland drift; The process of soft tissue being compressed by the puncture needle can be approximately regarded as the linear elastic deformation. So, the radial force received by the puncture needle gradually increases with the increase in puncture depth. Thus, the radial pressure on the part of the puncture needle penetrating the soft tissue can be approximated as a triangular distributed load. The puncture needle is always in a state of force balance during the uniform puncture process, and its overall forces analysis is shown in Figure 1.

In the z - x plane, o point in the bottom of the needle is the moment point, the puncture direction of the puncture needle is along the z axis, and the deflection direction is along the x axis. δ is the tip angle, F_z is the puncture force of the needle in the z axis, F_f is puncture friction, F_c is the shear force of the tip bevel, F_t is the friction of the tip bevel, q is the triangular load of the soft tissue acting on the needle body, L is the total length of the needle, L_0 is the length of the needle outside the soft tissue, M_{zx} is the puncture torque.

By analyzing the bending trend of the part of the puncture needle into the soft tissue, it can be known that the larger of the needle body deflection part, the larger of the soft tissue deformation it contacts. However, at any time during the puncture process, the axial force and radial force of the puncture needle will be balance. Therefore, as the puncture depth increases, the deflection of the puncture needle in the soft tissue will increase, and the force balance equation as:

$$\begin{cases} \sum F_z = F_z - F_c \sin \delta - F_t \cos \delta - F_f = 0 \\ \sum F_x = -F_t \sin \delta - q(L - L_0)/2 + F_c \cos \delta = 0 \\ \sum M = M_{zx} + q(2L^2 - 3L_0L^2 + L_0^3)/6(L - L_0) - F_c L \cos \delta = 0 \end{cases} \quad (1)$$

2) DEFLECTION EQUATION AND MOMENT

Through the force analysis when acupuncture soft tissues, it can be known that the puncture needle is deflected due to its interaction force inside the soft tissue. The deflection model of acupuncture soft tissue is shown in Figure 2. Where, I represents the ideal position of the needle, II represents the deflection position of the needle. In the z - x plane, z_1 is the theoretical needle axis, z_2 is the deflection needle axis, N_1 is the border line of soft tissue, N_2 is the vertical line perpendicular to the bevel of the needle tip during the needle

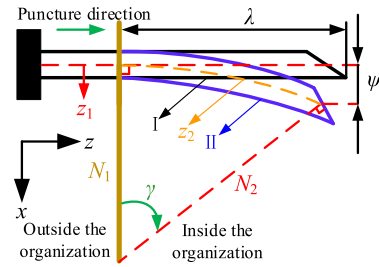


FIGURE 2. Deflection model diagram of acupuncture soft tissue.

is deflected, λ is the length of the puncture needle into the soft tissue, ψ is the deflection of the puncture needle, γ is the offset angle.

In the z - x plane, the bottom of the puncture needle is set to the origin of the coordinates, define the relationship between the deflection ψ of this point and the coordinate in the z direction as $\psi(\lambda)$, and combined with Figure 1 to get: $\lambda = L - L_0$; Where, L is the total length of the needle, L_0 is the length of the needle outside the soft tissue. Then, the relationship between the deflection and moment of this origin point and the deflection curvature of the needle is shown in formula (2):

$$\frac{1}{\rho} = -\frac{d^2\psi/dz^2}{[1 + (d\psi/dz)^2]^{3/2}} \approx \frac{M}{EI} \quad (2)$$

The puncture needle used in the interventional surgical treatment of soft tissue puncture of the prostate belongs to a semi-flexible alloy material. When the deflection of the needle shaft is too large, the material will fail and cannot be restored. At this time, the flexible needle have undergone plastic deformation. That is, the elastic modulus of the needle has changed. The equation (2) is the curvature equation of the flexible needle in the range of linear elasticity and pure bending. Where, ρ is the curvature of the needle, M is the total moment of the needle, E is the elastic modulus of the needle, I is the moment of inertia of the needle. According to equation (2), the deflection equation $\psi(z)$ of the puncture needle in the soft tissue of the prostate can be obtained, as shown in equation (3).

$$\psi(z) = -\frac{1}{EI} \int \left(\int M dz \right) dz \quad (3)$$

Due to the friction force F_t received at the needle tip bevel is smaller than the shear force F_c received at the needle tip bevel and the friction force F_f received by the needle body, the influence of F_t on the trajectory of the needle can be ignored. Therefore, through equation (1), the total bending moment when the puncture needle into soft tissue can be calculated as follows:

$$M = M_{bas} + M_{bar} \quad (4)$$

where, M_{bas} is the bending moment at the end of the needle, M_{bar} is the bending moment of the body of the puncture

needle; meanwhile, M_{bas} and M_{bar} are represented by equation (5) and equation (6) as:

$$M_{bas} = -F_c L \cos \delta + \frac{q(2L^2 - 3L_0L^2 + L_0^3)}{6(L - L_0)} \quad (5)$$

$$M_{bar} = [F_c \cos \delta - \frac{q(L - L_0)}{2}]z + \frac{q(z - L_0)^3}{6(L - L_0)} \quad (6)$$

3) NEEDLE DEFLECTION AND AFFECT FACTORS

It can be seen from equation (4) that the bending moment of the needle body when entering the soft tissue is affected by the shear force F_c of the needle tip bevel, the triangular load distribution force q received by the needle body and the puncture distance z . So, the equation (4) is inserted into the equation (3) to obtain the expression of the needle body deflection equation $\psi(z)$ when the puncture needle penetrates into the soft tissue, and the offset angle $\gamma(z) = \psi'(z)$. Then the deflection Angle of needle tip of puncture needle should be:

$$\phi(z) = \gamma(z) - \pi/4 \quad (7)$$

During the puncture operation, the trajectory of the boy of puncture needle is actually the trajectory that the needle tip passes through. When $z = L$, the deflection angle value of the puncture needle is determined by the variables F_c and q . Due to the small size of the bevel angle of the needle tip, the cutting and extrusion between it and the tissue is mainly the shear force perpendicular to the bevel, and the friction force parallel to the bevel is extremely small. Therefore, the influence of the friction F_t of the tip bevel on its deflection angle can be ignored in the puncture analysis.

Because the friction F_f on the needle body is relatively large, according to the force analysis when the puncture needle into the soft tissue, the friction F_f on the needle body can be approximately expressed as: $F_f = \mu q(L - L_0)/2$; Where, μ is the friction coefficient between the needle and the soft tissue, and from equation (1), F_c and q can be expressed as:

$$q = \frac{F_c L \cos \delta - M_{yx} \sin \delta}{\frac{\mu(L-L_0)L \cos \delta}{2} + \frac{(2L^2 - 3L_0L^2 + L_0^3) \sin \delta}{6(L-L_0)}} \quad (8)$$

$$F_c = \frac{2F_z - \mu q(L - L_0)}{2 \sin \delta} \quad (9)$$

Incorporating equations (8) and (9) into equation (7), the relationship between the deflection angle ϕ of the puncture needle, the puncture force F_z , and the puncture moment M_{zx} can be obtained when $z = L$. Because the puncture needle is fixed on the base at the end of the robot, the influence of the puncture torque M_{zx} can be ignored.

When the puncture needle enters the soft tissue at a constant speed, its puncture force F_z is approximately equal to the sum of the friction force F_f received by the needle body and the shear force F_c received by the needle tip bevel. Among them, the value of F_c is related to the geometric parameters of the puncture needle and the stiffness of soft tissue, and for

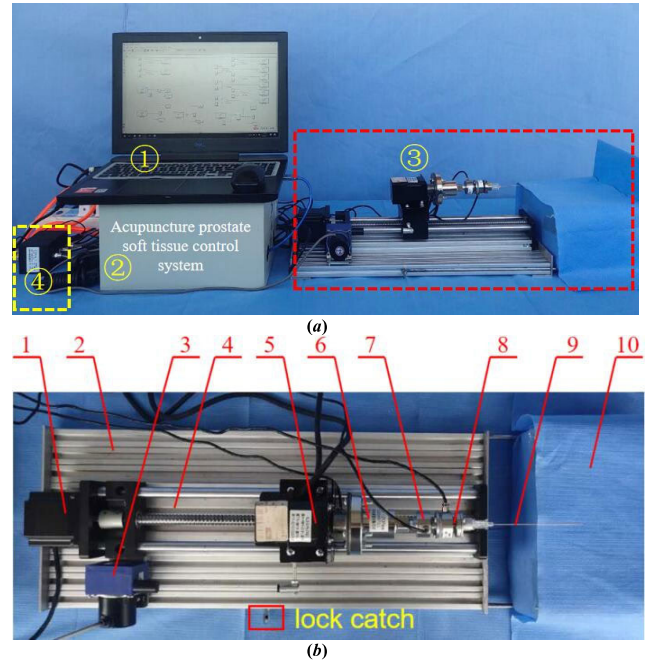


FIGURE 3. The test platform. (a) System structure, (b) Executive mechanism. Where, 1. Servo motor A; 2. Support base; 3. Pull wire displacement sensor; 4. Linear sliding table; 5. Servo motor B; 6. 6D force sensor; 7. Pressure Sensor; 8. Torque sensor; 9. Medical surgical seed implantation puncture needle; 10. Soft tissue placement bracket.

the same puncture needle and soft tissue, the cutting force can also be expressed as a constant ($F_c \ll F_f$).

Therefore, during the prostate seed implantation puncture operation, there is a relatively large frictional F_f between the needle body and the soft tissue to increase the puncture force F_z , which in turn leads to a large deflection of the puncture needle during puncture, which seriously affects the accuracy of puncture positioning.

B. TEST PLATFORM

Combined with the above analysis, in order to overcome the problem of poor positioning accuracy caused by the puncture friction when acupuncture soft tissues, it was necessary to study a puncture control method for prostate soft tissue to reduce puncture friction, which was a key factor to effectively reduce the deflection angle of puncture needle and ensure the puncture accuracy.

Therefore, for the follow-up theoretical research and experimental analysis of prostate soft tissue puncture control methods, it was necessary to design and build a prostate soft tissue puncture test platform that meets its performance requirements. This section will introduce the test platform in detail according to its structure, function and working principle.

1) STRUCTURE AND FUNCTION

As shown in Figure 3(a), the overall system of acupuncture prostate soft tissue test platform consists of the following three parts: ① Computer, ② Acupuncture prostate soft tissue control system, ③ Executive mechanism and ④ Amplifier.

The laptop as the upper computer, its control operation interface and monitoring interface was written by Matlab-2016a/Simulink, and it was mainly responsible for sending control commands, logic algorithm, data processing, data transmission, data storage and data monitoring.

Acupuncture prostate soft tissue control system was used as the lower computer, used the Advantech PC104 industrial control board as the core controller. Its computing system adopted XPC system, which can be well compatible with computers and be embedded in Matlab/Simulink and related modules, and its computing speed is fast, and it is used to control the puncture movement of puncture needle, collect the position and the signal collected by force sensor, and communicate with the upper computer. The peripheral hardware components of the control system include: (1) HIT-PC104-HXL-P515 acquisition card, which is used for the acquisition of displacement sensor and force sensors information and A/D conversion; (2) HIT-PC104-HXL-P520 is used for D/A conversion to generate the drive control signal of the servo motor and transmit it to the servo drive; Among them, each board driver program adopts Matlab-2016a to write S-Function module through embedded C++.

The executive mechanism is mainly used to complete the puncture operation of the soft tissue, and its composition structure is shown in Figure 3(b). Servo motor A is responsible for the drive of needle insertion and withdrawal, servo motor B is responsible for the rotation drive of the puncture needle (Considering the winding situation, the circumferential rotation of the needle needs to be equipped with a dual-axis DC rotating reduction motor in front of the torque sensor); The pull wire displacement sensor is fixed on the side end of the sliding block on the linear sliding table, which is used for closed-loop control of the linear position and transfer of needle position data; The 6D force sensor is fixed on the axis of the servo motor B, which is mainly used for force closed-loop control (It realizes force/position fusion control together with the displacement sensor, which can ensure the positioning accuracy of the puncture needle), and it is compared and analyzed with the data returned by the pressure sensor and torque sensor; The soft tissue placement bracket is installed on both sides of the supporting base through its bottom two rods and can slide, so as to realize free adjustment of puncture test samples. After the adjustment, the bracket is locked and fixed through its side end lock.

2) WORKING PRINCIPLE

The working principle diagram of the acupuncture prostate soft tissue test platform is shown in Figure 4. Meanwhile, the pink background part represents the upper computer software operating system, and the gray background part represents the lower computer hardware and execution system; At the same time, with the green dotted line as the boundary, the upper part is the rotation drive system of the puncture needle, and the lower part is the needle insertion and withdrawal system of the puncture needle.

In the upper computer software operating system, a is the input signal of the puncture needle rotation drive, b is the input signal of the puncture needle drive, c/d are the tracking expectation (In Figure. 4, the force controllers respectively represent the needle advancement driving force controller and the rotation driving force controller; So the definition c is the desired needle advancement driving force and d is the desired rotation driving force), e is the rotary drive position ring, f is the rotating drive speed ring, g is the needle drive speed loop, h is the needle drive position ring, i are the direction component of the forward/retract needle in the six-dimensional force sensor, j is the torsional moment in the six-dimensional force sensor (In Figure 4, the torsion torque is transmitted from the send_T to the receive_T).

In the lower computer and executive mechanism system, ① means servo motor driver B, ② means servo motor driver A, ③ means the displacement sensor acquisition channel, ④ means the acquisition channel of the torque sensor, ⑤ means the acquisition channel of the pressure sensor, ⑥ means the acquisition channel of the 6D force sensor. Meanwhile, the two modules “HXL-520 Analog Output” and “HXL-515 DIO Input” shown in Figure 4 represent the hardware part and the S-Function driver module written by Matlab-2016a.

In the soft tissue puncture test, the puncture needle drive signal is input from the b channel (Ramp response signal), and then reaches the HIT-PC104-HXL-P520 drive through the position loop h and the velocity loop g , which can realize variable speed movement and accurately track the position input curve; At the same time, its corresponding hardware outputs a voltage analog signal of 0V~10V to servo driver A, and drives the executive mechanism to complete the puncture task. The working principle of the rotary puncture drive is the same as that of the puncture drive. In order to ensure the positioning accuracy during the puncture test, both the needle insertion drive and the rotation drive adopt the force and position fusion control as shown in Figure 4, which meets the performance requirements of the test platform in the follow-up test research. During the test, the displacement and force data collected by the actuator are observed and recorded by Target Scope1 and Target Scope2.

III. PUNCTURE METHOD BASED ON SINE ROTATION

When the robot is performing soft tissue puncture, the soft tissue has a great friction force on the puncture needle, so that the puncture robot needs to provide a large puncture force. The conclusions from the theoretical analysis in Section 2 showed that if the direct needle insertion method was used to puncture the soft tissues, the puncture needle would have the larger deflection. Therefore, it was necessary to conduct in-depth research on its puncture method to reduce the deflection angle of the puncture needle when it entered the soft tissue and improved its puncture accuracy.

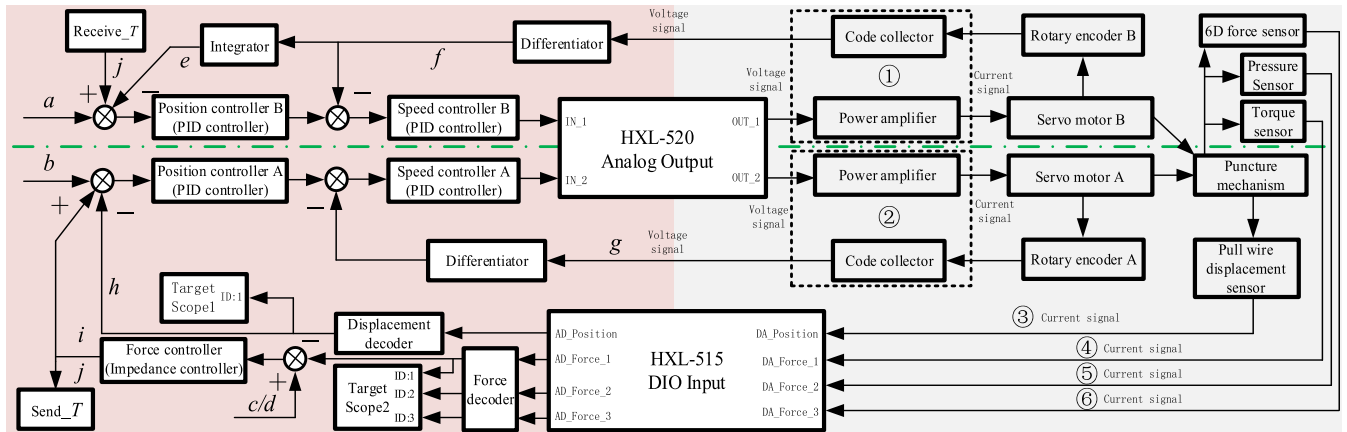


FIGURE 4. Working principle diagram of acupuncture prostate soft tissue test platform.

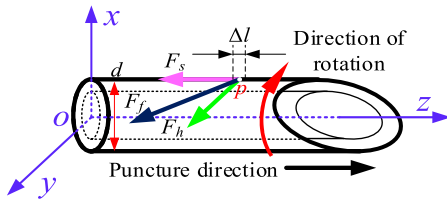


FIGURE 5. Rotating puncture model diagram.

A. ROTATING PUNCTURE METHOD

In the process of prostate soft tissue puncture, the main purpose of rotating puncture was to improve the accuracy of puncture positioning [15], [24], [30]. In addition, when the doctor manually punctures the patient, since the skin and flesh tissue of the human body will generate greater friction on the puncture needle, the rotation of the needle can reduce the work intensity of the doctor’s operation. Therefore, in various methods of soft tissue puncture, it was necessary to conduct a systematic analysis of the puncture method of rotating needle. So, according to the analysis in Section 2, the mechanical model of rotating soft tissue puncture was established as shown in Figure 5:

In the coordinate system $oxyz$, Δl is a micro element on the axis of the puncture needle, p is a point within Δl , F_s is the friction component of point p along the z axis, F_h is the circumferential friction component of point p (its direction is constantly changing in the xoy plane), F_f is the resultant force of friction at point p , d is the diameter of the needle shaft.

It can be seen from Figure 5 that the puncture needle performs needle insertion and rotation along the z axis in the coordinate system $oxyz$. In the case of ignoring the tangential force and hardness force generated by the needle tip and the soft tissue, set a micro-element on the shaft surface of the puncture needle as Δl , and a point p in Δl represents the force of the entire micro-element. When the puncture needle enters the soft tissue at a constant speed (Under the condition of constant power), the friction on the needle entering the tissue

can be expressed as:

$$\sum F_f = \pi d \int_0^l \sqrt{F_s^2 + F_h^2} \Delta l \tag{10}$$

where, $\sum F_f$ is the total friction force of the needle entering the soft tissue part; Its value could be approximated to a constant value at a fixed depth of the same soft tissue [24].

So, according to equation (10), if the soft tissue puncture is performed by the direct needle insertion method, F_h is 0, the total friction of the needle entering the soft tissue part is expressed as:

$$\sum F_f = f(F_s) \tag{11}$$

Therefore, through the analysis of equation (10) and equation (11), it can be known that the method of rotating the needle can effectively reduce the axial friction (Puncture resistance) of the puncture needle when it penetrates into the soft tissue and improve the accuracy of puncture positioning.

1) CIRCUMFERENTIAL ROTATION PUNCTURE

In order to solve the problem of needle tip deflection caused by the large friction generated by the doctor when puncturing the soft tissue, according to the literature [24], some researchers mainly used the circumferential rotation puncturing method for soft tissue puncture, and its specific rotating puncture model as shown in Figure 6.

It can be seen from Figure 6 that the circumferential rotation puncture method uses the puncture needle to make continuous circumferential rotation around its central axis A. The rotation direction does not change with time, but the rotation angle changes continuously with time (The rotation angle is continuously superimposed with the continuous changes of $t_1, t_2, \dots, t_{n-1}, t_n$), so the rotation angle of the needle tip changes linearly with time. Therefore, combined with the analysis of formula (10), it can be seen that the circumferential rotation puncture soft tissue is to increase

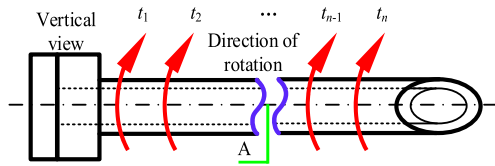


FIGURE 6. Circumferential rotation puncture model.

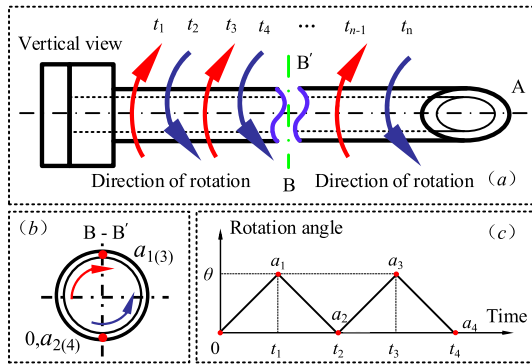


FIGURE 7. Alternate rotation puncture model. (a) Vertical view, (b) B-B' section drawing, (c) Rotation angle change graph.

the circumferential friction of the puncture needle through uniform circumferential rotation, thereby reducing its axial friction and achieving the purpose of reducing the deflection angle of puncture needle into soft tissue, so as to complete the precise positioning of soft tissue puncture surgery.

2) ALTERNATE ROTATING PUNCTURE

Alternate rotation puncture was a new type of rotation needle insertion method proposed by Majewicz A et al. [26] in 2014. This puncture method is more in line with the manual rotation needle insertion operation. The specific rotation model is shown in Figure 7.

It can be seen from Figure 7(a) that the alternately rotating puncture method uses the puncture needle to reciprocate and rotate around its axis A, and its rotation direction changes with time ($t_1, t_2, t_3, t_4 \dots t_{n-1}, t_n$) continuous change. As shown in Figure 7(b), observe the cross-section B-B' of the needle, with the needle tip as the marking point and indicated by the red dot (Temporarily recorded as $a_i, i = 1 \sim 4$; initial position is recorded as 0); The rotation time t of the puncture needle is from 0 to t_1 , and the rotation angle of the puncture needle changes θ as a_1 . When the rotation time t of the puncture needle is from t_1 to t_4 , the rotation angle of the puncture needle $a_1 \sim a_4$ alternately changes from θ to 0 (Where, $0 < \theta \leq 2\pi$, tentatively designated as π), and follow the rotation method shown in the cross-sectional view of Figure 7(b) and so on; Therefore, the rotation angle of the needle tip changes periodically with time, so the change in the speed of alternate rotation can be expressed by frequency.

As shown in Figure 7(c), the angle change of two cycles is shown, and the rotational torque of the puncture needle in the tissue is consistent with the angle change.

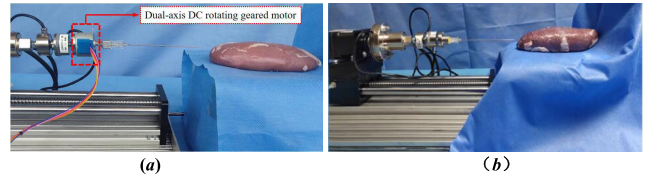


FIGURE 8. Test device. (a) Circumferential rotational puncture, (b) Alternate rotating puncture.

3) THEORY TEST I

Through the analysis of equation (10), it could be seen that the friction force generated by the puncture needle entering the soft tissue increases with the increase of the puncture depth, and due to the large damping inside the human soft tissue; Therefore, it was assumed that its circumferential friction force was puncture depth and rotation speed were related. So, in order to verify the effectiveness of the rotary puncture method in reducing puncture friction, it was necessary to conduct theoretical tests on its circumferential and alternate rotary needle insertion methods.

a: TEST DEVICE

As shown in Figure 8(a), it is a test device for circumferential rotation of the needle. It is based on the test equipment of Figure 3(b), and a dual-axis DC rotating geared motor is installed on the torsion sensor; The test device shown in Figure 8(b) is consistent with Figure 3(b).

b: TEST OBJECT

In the human urinary system, different tissues and organs have different elastic differences; when these tissues become cancerous, the change of internal composition of soft tissue will also cause the change of elastic modulus. Since prostate soft tissue puncture is a minimally invasive surgery of the urinary system, according to the design requirements of the puncture machine for radioactive seed implantation treatment of prostate cancer, in order to ensure the accuracy of the test, it is necessary to select representative test objects (Such as the kidney and other urinary organs in large mammals [30]). First, according to the shear wave elastography technology [33], real-time tissue elastography ultrasound diagnostic equipment was used to determine the elastic modulus of the kidney organs of different types of large mammals (Such as pigs, cattle, sheep, etc.). The results are shown in Table 1.

Then, the measured data obtained from Table I was compared with the elastic modulus of prostate tissue with cancer measured according to the document [33] (First, subtract the value of H-L with other samples, and then compare its values). The elastic modulus (E_{max}, E_{mean}) of pig kidney at room temperature was similar to that of the prostate elastic modulus of the prostate cancer patients, so pig kidneys were selected for testing samples.

Since the prostate soft tissue is in a free state in the human body, it cannot be fixed during the actual puncture operation. So the test sample was not fixed during the test;

TABLE 1. Elastic modulus value of the sample to be tested.

category	Number	E _{max} (kPa)	E _{mean} (kPa)
P-k	30	82.92±19.32	72.82±16.74
B-k	20	73.43±26.04	64.97±26.03
S-k	16	58.35±11.83	40.36±13.54
H-k	6	70.20±17.65	40.36±13.54
D-k	4	61.57±20.21	40.36±13.54
H-L	—	88.76±25.15	79.59±25.86

Elastic modulus can well reflect the mechanical properties of material deformation, and is often used in the detection of prostate cancer [33], [34]. P-k = Pig kidney, B-k = Bovine kidney, S-k = Sheep kidney, H-k = Horse kidney, D-k = Deer kidney, H-L is the prostate elastic modulus of the prostate cancer patients described in literature [33].

c: TESTING METHOD

Including circumferential friction test and puncture resistance test (Where, the puncture resistance is equal to the puncture force F_z). In addition, The three sets of parameter values in the circumferential friction test and the axial puncture resistance test were all selected in combination with the reference data range provided by surgeons with rich clinical minimally invasive puncture surgery experience in Hailun People’s Hospital, Heilongjiang Province, China.

d: CIRCUMFERENTIAL FRICTION TEST

Circumferential and alternating rotation puncture both adopted a needle insertion speed of 11.25mm/s for pig kidney puncture, and the puncture depth was 0mm~80mm; Where, according to the performance of the geared motor, the torque output of the puncture needle in the soft tissue was guaranteed to be good, so the rotation speed of the circumferential rotation needle was selected as [0, 30, 60, 90, 120]rad/min. At the same time, the rotation frequency of alternately rotating puncture should correspond to the circumferential rotating puncture speed. Therefore, when the rotation angle was $\theta = \pi$, the rotation frequency of alternately rotating should be [0,0.5,1.0,1.5,2]Hz. When the alternate rotation speed or circumferential rotation speed was 0, it means direct puncture.

e: AXIAL PUNCTURE RESISTANCE TEST

The puncture speed of circumferential and alternate rotation was 11.25mm/s; Where, in the test of the same rotation speed/frequency and different puncture depths, and the circumferential rotation speed was 90rad/min, the alternate rotation frequency was 1.5Hz, and the needle penetration depth was 0mm~70mm; In the same puncture depth and different speed (Frequency) tests, the puncture depth was 70mm, the circumferential rotation speed was 0rad/min~105rad/min, the alternating rotation frequency was 0rad/min~1.75Hz, the rotation angle is $\theta = \pi$.

f: TEST RESULTS

g: CIRCUMFERENTIAL FRICTION TEST

In order to ensure that the test results obtained were universal and general, a total of 40 groups of experiments

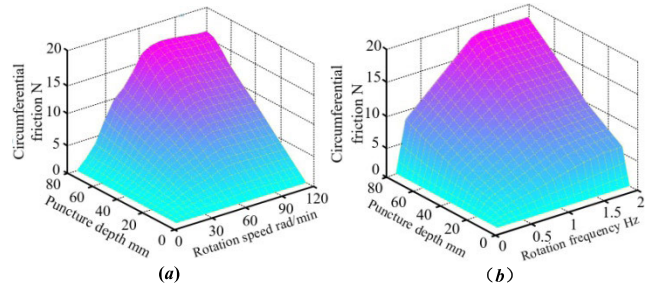


FIGURE 9. The test drawing of circumferential friction. (a) Circumferential rotation, (b) Alternate rotating.

were performed by rotating and alternating puncture, each group was repeated for 3 times, took the maximum value of the data in each test process and calculated the average value of the maximum value of three repeated tests. In addition, the test results of alternate rotation puncture would be combined with Figure 7(c), the values of rotation moments corresponding to the angles (a_1 and a_3 , etc.) at t_1 and t_3 were selected. Meanwhile, according to the average value of the rotation torque, and the circumferential friction was calculated approximately by equation (12). The test result is shown in Figure 9.

$$F_h = T_h/r \tag{12}$$

where, T_h is the torque of rotation; r is the cross sectional radius of the puncture needle.

h: AXIAL PUNCTURE RESISTANCE TEST

In order to ensure that the test results obtained were universal and general, a total of 25 tests were conducted with direct puncture, circumferential puncture and alternately rotating puncture. Each group was performed for 3 times, took the maximum value of the data in each test process and calculated the average value of the maximum value of three repeated tests. The test results of the axial puncture resistance were shown in Figure 11.

i: RESULT ANALYSIS

1) It can be seen from Figure 9 that the puncture needle is in the soft tissue, both the puncture depth and the rotation speed affect the size of the circumferential friction, and the circumferential friction increases with the increase of the puncture depth and rotation speed; It means that the deeper the puncture needle enters the soft tissue, the faster the rotation speed, and the greater the pressure and damping force of the soft tissue on the needle body.

According to Figure 9(a), it can be seen that in the circumferential rotation puncture method, the circumferential friction force increases linearly with the puncture depth and rotation speed, but as the rotation speed of the puncture needle increases to 60rad/min, the circumferential friction become stable after reaching 17.5N (Not increasing); The reason was: As shown in the figure 10, as the rotation speed increases (Over 60rad/min), the rotational kinetic energy of the puncture needle loaded into the soft tissue increases,

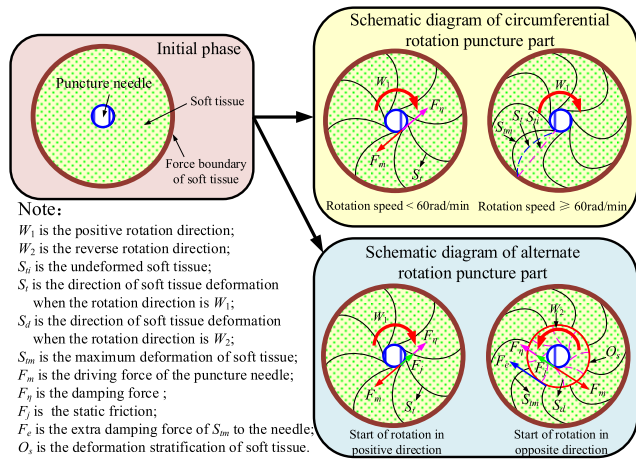


FIGURE 10. Schematic diagram of rotating puncture analysis.

FIGURE 10. Schematic diagram of rotating puncture analysis.

but, due to the viscous properties and strain limit of the soft tissue itself, the deformation (S_i to S_{m1}) of the soft tissue driven by the needle body in the rotation direction reaches the maximum value (The circumferential rotational friction is equal to the damping force F_{η}), which makes the puncture the needle overcomes the maximum damping force of the soft tissue on it and gradually maintains stable.

Meanwhile, it could be seen from Figure 9(b) that the performance of the alternating rotation puncture method and the circumferential rotation puncture method are basically the same. When the rotation frequency was less than 0.3Hz, the circumferential friction increased quickly, and the rotation frequency was 0.3Hz~1.2Hz, and the circumferential friction increased steadily, but as the alternating rotation frequency increases to 1.2Hz, the trend of its circumferential friction begins to increase slowly after 1.2Hz; The reason was: As shown in the figure 10, as the rotation frequency increases, the kinetic energy of the puncture needle also gradually increases, but as the direction of rotation changes (W_1 to W_2), the rotation of the puncture needle was temporarily stopped and gradually accelerated, resulting in a deformation stratification (O_s) of the soft tissue (When the puncture needle changed the direction of rotation, the soft tissue near the needle body deforms firstly (S_d), the soft tissue away from the needle body remains unchanged (S_{m1}) and there is a damping force, so there is stratification between S_{m1} and S_d , which made the puncture needle need to overcome its extra reverse damping force (F_e). When the rotation frequency is less than 0.3Hz, the circumferential friction is the static friction (F_j); When the rotation frequency is 0.3Hz~1.2Hz, the static friction (F_j) gradually increases, but it does not reach the maximum value; When the rotation frequency exceeds 1.2Hz, in the initial stage of movement, the puncture needle has a large rotational inertia due to the increase in frequency, and the existence time of static friction can be ignored, so the circumferential friction directly transitions to dynamic friction force (Equal to F_{η}).

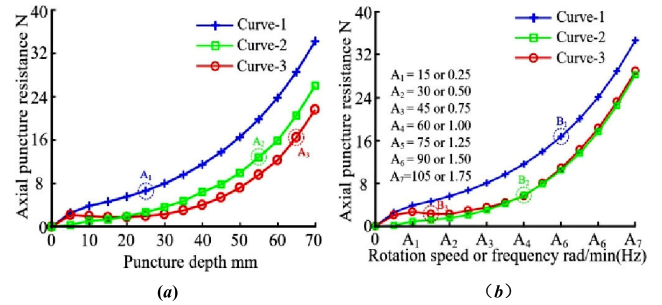


FIGURE 11. Axial puncture resistance test. (a) Different puncture depth, (b) Different rotation speed or frequency. Where, Curve-1 is the curve of direct puncture; Curve-2 is the curve of circumferential rotation puncture; Curve-3 is the curve of alternate rotation puncture.

Therefore, the effect of alternate rotation puncture is better than that of circumferential rotation puncture; When the alternating rotation frequency reaches 2Hz (corresponding to 120rad/min shown in Figure 9(a)), the peak value of its circumferential friction reaches 18.6N (It is slightly more than 17.6N, indicating that its rotation angle has not reached the maximum deformation of soft tissue, so the choice of rotation angle cannot be too small).

2) In Figure 11 (a), A_1 is the point of maximum deviation in the direct puncture curve (Where, the three values of the point are 7.05N, 6.87N, 6.03N, the average value is 6.65N, and the deviation between the maximum and the minimum value is 1.02N); A_2 is the point of maximum deviation in the circumferential rotation puncture curve (Where, the three values of the point are 12.93N, 12.47N, 11.85N, the average value is 12.75N, and the deviation between the maximum and the minimum value is 1.08N); A_3 is the point of maximum deviation in the alternate rotation puncture curve (Where, the three values of the point are 16.77N, 16.62N, 16.11N, the average value is 16.50N, and the deviation between the maximum and the minimum value is 0.66N). In Figure 11 (b), B_1 is the point of maximum deviation in the direct puncture curve (Where, the three values of the point are 16.74N, 16.48N, 16.22N, the average value is 16.48N, and the deviation between the maximum and the minimum value is 0.52N); B_2 is the point of maximum deviation in the circumferential rotation puncture curve (Where, the three values of the point are 6.37N, 6.24N, 5.60N, the average value is 6.07N, and the deviation between the maximum and the minimum value is 0.77N); B_3 is the point of maximum deviation in the alternate rotation puncture curve (Where, the three values of the point are 2.66N, 2.15N, 1.58N, the average value is 2.13N, and the deviation between the maximum and the minimum value is 1.08N).

Therefore, the data shown in Figure 11 can express the universality and generality of the test results.

From the test results shown in Figure 11, it can be seen that in the initial stage of puncture and rotation, the alternate rotation puncture method cannot effectively reduce the puncture resistance.

The fundamental reason is: Combined with the analysis of Figure 9(b), when the puncture needle begins to

perform puncture or rotation, the circumferential friction quickly increases, causing the soft tissue to deform, this will cause friction adhesion, entanglement and wrapping between the soft tissue and the puncture needle. The puncture effect is similar to the direct puncture method. From the test results shown in Figure 11(a), it can be seen that as the depth of needle insertion increases, although both circumferential and alternating rotation puncture methods can reduce puncture resistance, the effect of alternating rotation needle insertion is more obvious. Meanwhile, the analysis of the test results in Figure 11(b) and Figure 9 shows that when the puncture depth is the same, with the increase of the circumferential rotation speed and the alternating rotation frequency, their puncture resistance value is significantly reduced compared to the direct puncture method; But, between A_2 and A_3 , the puncture resistance values of the two rotation methods are approximately the same. Between A_3 and A_5 , the effect of alternate rotation puncture is more obvious than that of circumferential rotation puncture. Between A_5 and A_7 , the effect of alternately rotating the needle is similar to that of rotating the needle in the circumferential direction (The axial puncture resistance of alternating rotation puncture is slightly lower than that of circumferential rotation puncture). Therefore, the puncture resistance test verifies the circumferential friction test results.

Through the above test analysis, it can be known that if the puncture operation requires deep puncture, circumferential and alternate rotation puncture methods cannot effectively guarantee the puncture effect.

j: EXISTING PROBLEMS

When the circumferential and alternating rotation puncture methods are used for puncture operations, although theoretical analysis has proved its feasibility and is superior to direct puncture methods; But, in the actual test operation process, both puncture methods have problems. As shown in Figure 12(a), the circumferential rotation punctures the soft tissue. During the puncture process, the puncture needle and the soft tissue are likely to cause entanglement, which affects the puncture accuracy; Therefore, during the test, the test object needs to be fixed by hand or other clamping mechanism, as shown in Figure 12(b).

Figure 12(c) shows the side view of alternately rotating puncture. When the positive direction of the needle tip bevel is upward as the initial rotating puncture position, according to the test methods for puncture test, and puncture needle and yellow line (Horizontal line) approximately parallel. It shows that the alternate rotation needle insertion method can effectively improve the deflection problem caused by direct puncture. However, it can be seen from the top view that this method of puncturing soft tissues is easy to cause lateral drift and compression deformation, as shown in Figure 12(d).

So, the circumferential and alternating rotation puncture methods are only suitable for the fixed visceral tissues of the human body or the minimally invasive puncture operations

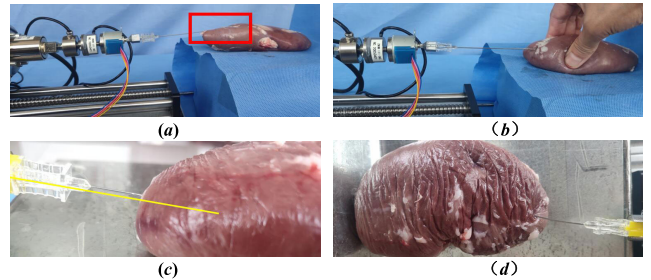


FIGURE 12. Problems in circumferential and alternating rotation puncture methods. (a) The entanglement between the needle and the soft tissue during circumferential rotation puncture (Where, The red area indicates entanglement between the needle and the soft tissue), (b) Need to hold the target soft tissue during circumferential rotation puncture, (c) Side view of alternate rotation puncture (The yellow line is the horizontal line), (d) Vertical view of alternate rotation puncture.

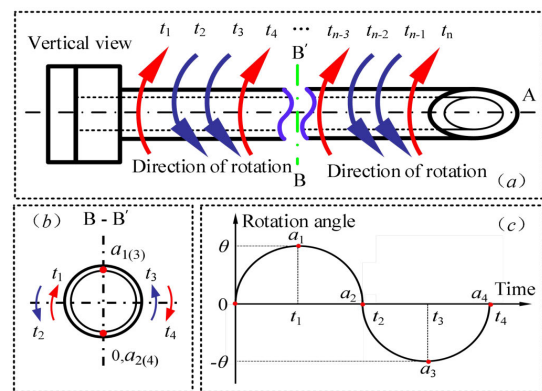


FIGURE 13. Sine rotation puncture model. (a) Vertical view, (b) B-B' section drawing, (c) Rotation angle change graph.

that are easy to perform external fixation, and the puncture movement needs to adopt an intermittent control method. Since the prostate is a suspended organ tissue in the human body, it is necessary to design a continuous needle control method suitable for prostate soft tissue puncture for minimally invasive surgery of prostate seed implantation.

B. SINE ROTATION PUNCTURE METHOD

According to the above analysis, it can be seen that when performing prostate soft tissue puncture surgery, the use of rotary puncture compared with direct puncture, these two puncture methods can effectively reduce the puncture friction and increase the puncture deflection angle. The two puncture methods can effectively reduce the puncture friction and reduce the puncture deflection angle. However, by analyzing and comparing the two existing rotary puncture methods, due to many shortcomings, they cannot guarantee the puncture accuracy. So, this paper proposed a sine rotation puncture control method.

1) SINE ROTATION PUNCTURE THEORY

The theory of sine rotation puncture is based on the principle of rotation puncture, and its rotation model is shown in Figure 13(a). The sine rotation puncture method is to rotate

the puncture needle in a reciprocating sine swing around its axis A, and its rotation direction changes with time ($t_1, t_2, \dots, t_{n-1}, t_n$). As shown in Figure 13(b), observe the needle's cross-section B-B', use the needle tip as the marking point and indicate it with a red dot (Temporarily recorded as $a_i, i = 1 \sim 4$; initial position is recorded as 0), the rotation time t of the puncture needle is from $0 \sim t_1$, and the rotation angle θ of the puncture needle is recorded as a_1 . When the rotation time t of the puncture needle is from t_1 to t_4 , the rotation angle $a_1 \sim a_4$ of the puncture needle changes from θ to 0 in a sine cycle (Where $0 < \theta \leq 2\pi$, tentatively set as π), and the rotation mode of each cycle as shown in the cross sectional view of Figure 13(b), and so on.

Therefore, the rotation angle of the needle tip changes in a sine cycle with time, and its rotation rate can also be expressed by frequency, as shown in Figure 13(c) for its 1-cycle angle change. So, the angle rotation equation of the sine rotation puncture model is:

$$\theta_i = \alpha \cdot \sin(\beta \cdot t) + b \tag{13}$$

where, θ_i is the current rotation angle, α is the amplitude of the rotation angle, β is the sine rotation frequency, t is the running time, b is the initial angle of rotation of the puncture needle (The position where the bevel of the needle tip facing upward, and b is defined as 0°).

According to equation (13), it can be seen that when sine rotation is used to puncture the soft tissue of the prostate, the angular velocity and angular acceleration and the direction can change continuously with time, and the rotation angle, angular velocity and angular acceleration of the puncture needle are rotated to near the extreme value, it can ensure its excessive smoothness and stability.

Compared with the circumferential and alternating rotation puncture, the output power and output torque of the servo motor are reduced while satisfying the reduction of puncture friction, and the oscillation can be effectively relieved during the high-frequency sine rotation puncture, thereby reducing the impact damage to local soft tissues to improve puncture accuracy.

At the same time, under the same rotation frequency, the change angle of sine rotation is greater than the change angle of alternate rotation, which can effectively increase the circumferential friction of the puncture needle and reduce the axial puncture resistance.

2) SINE ROTATION THEORY TEST

In order to verify the validity and rationality of the sine rotation puncture theory, the circumferential friction force and axial puncture resistance of puncture needle should be tested. The test device, test object and test method during the test are consistent with the previous part. In order to keep the speed of sine rotation correspond to that of circumferential and alternating rotation the same, the frequency of sine rotation as $[0,0.25,0.5,0.75,1]$ Hz, and the puncture speed for circumferential friction and axial puncture resistance tests as 11.25mm/s. The axial puncture resistance test used the sine

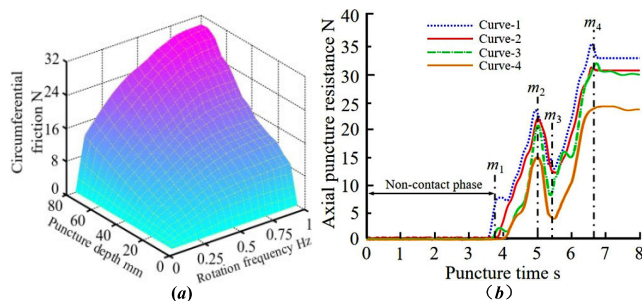


FIGURE 14. Sine rotation puncture theory test. (a) Circumferential friction test, (b) Axial puncture resistance test (Curve-1 is the curve of direct puncture; Curve-2 is the curve of circumferential rotation puncture; Curve-3 is the curve of alternate rotation puncture; Curve-4 is the curve of sine rotation puncture).

rotation puncture method and the circumferential rotation puncture, the alternate rotation puncture, the direct puncture methods for comparative analysis. The tests results is shown in Figure 14.

It can be seen from Figure 14(a) that the circumferential friction force is significantly greater than the circumferential rotation puncture and the alternate rotation puncture when the sine rotation is used to puncture the soft tissue, but as the rotation frequency increases, its circumferential friction gradually increases; When the puncture depth and rotation frequency reach the maximum, the circumferential friction force reaches 31.2N, and there is a tendency to continue to increase. The reason was the same as the alternate rotation puncture method, but within one rotation cycle, the soft tissue deformation was approximately twice that of the alternate rotation, so the circumferential friction (damping force) received by the puncture needle was also much larger than greater than the alternate rotation method; In addition, when the rotation direction is changed at the extreme point, the speed change (deceleration/acceleration) near the extreme point is continuously and smoothly, which can effectively suppress the rotational inertia of the puncture needle when the rotation frequency is too fast, this can slow down its premature arrival of dynamic friction. So, combined with equation (10), it can be seen that the axial puncture resistance can be effectively reduced; Which shows that the sine rotation needle insertion method is better than the other two needle insertion methods.

Figure 14(b) shown the complete data results of the axial puncture resistance test were completed by the four puncture methods; among them, each puncture method only performs the puncture soft tissue test process once. Meanwhile, the line segment m_1 is the initial stage when the puncture needle contacts the soft tissue, the line segment m_2 is the stage when the puncture needle just pierced the soft tissue, the line segment m_3 is the buffer stage after the puncture needle pierces the soft tissue, the line segment m_4 is the stop stage of the puncture needle, and the puncture time is 8s.

According to the puncture results shown in Figure 14(b), it can be seen that the use of sine rotation to puncture soft tissue can effectively alleviate its axial puncture resistance. At the same time, combining Figure 15 and Figure 12 shows

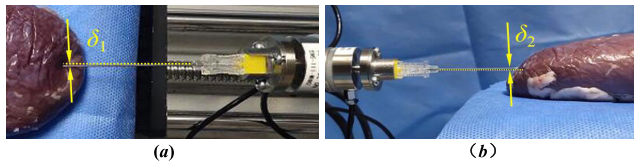


FIGURE 15. The effect of sine rotation puncture (The yellow line is the horizontal line. δ_1 is the lateral deflection angle, δ_2 is the longitudinal deflection angle); (a) Vertical view, (b) Side view.

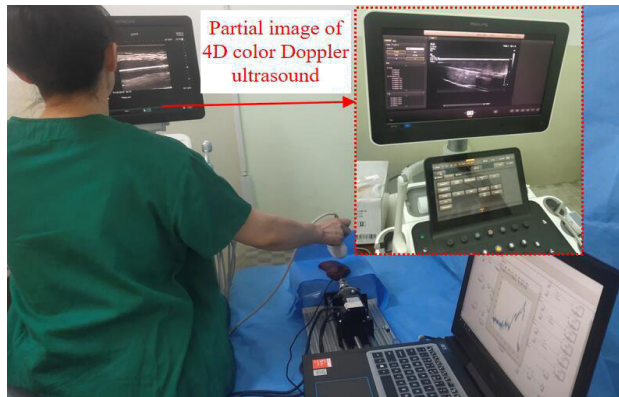


FIGURE 16. Performance comparison test process.

that the puncture effect of sine rotation is significantly better than the other three puncture methods, and it can effectively inhibiting the axial puncture resistance, thereby reduce the extrusion and deformation between the puncture needle and the soft tissue in the puncture direction, and ensure the continuity of puncture control. However, it can be seen from the vertical view and the side view that there are still deflection angles δ_1 and δ_2 between the puncture needle and the marked yellow line.

The test results of the sine rotation puncture theory show that the sine rotation puncture can ensure the continuous deep puncture and the need for puncturing the suspended organs and tissues in the human body.

C. PERFORMANCE COMPARISON TEST

In order to further verified the validity of the above analysis theory and the feasibility of the sine rotation puncture method when the puncture needle entered the soft tissue, it was necessary to conduct a performance comparison tests. The test site was in the Department of Imaging, Hailun People’s Hospital, Suihua City, Heilongjiang Province, China. The test instrument used the Philips ECIQ7-4D color Doppler ultrasound, as shown in Figure 16.

The test device as shown in Figure 3; Test sample as the pig kidney; The test parameters were selected as follows: puncture speed as 11.25mm/s, rotation speed (Frequency) as circumferential rotation was 90rad/min, alternating rotation was 1.75Hz and sine rotation was 0.75Hz, rotation angle as 180°; The test principle: Compared the sine rotation puncture method with direct puncture method, circumferential rotation

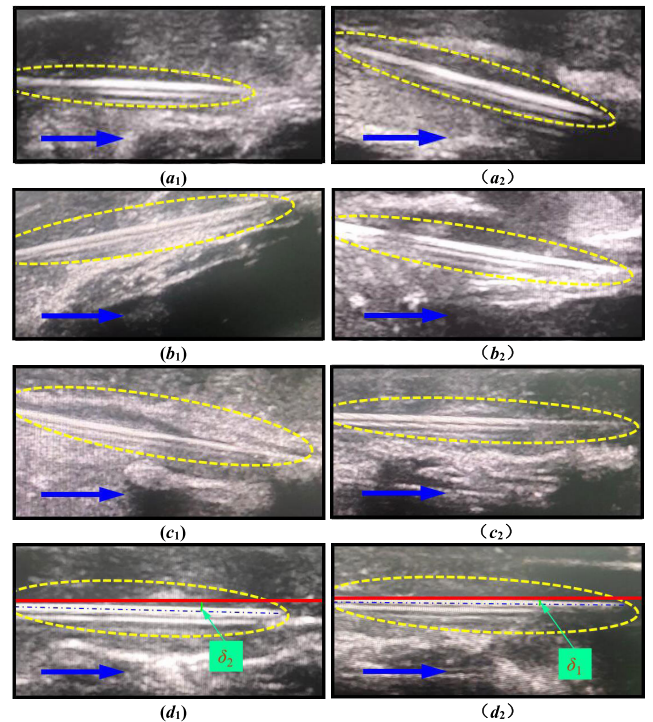


FIGURE 17. Performance comparison analysis test. (a₁) Vertical view of direct puncture, (a₂) Side view of direct puncture, (b₁) Vertical view of circumferential rotation puncture, (b₂) Side view of circumferential rotation puncture, (c₁) Vertical view of alternate rotation puncture, (c₂) Side view of alternate rotation puncture, (d₁) Vertical view of sine rotation puncture, (d₂) Side view of sine rotation puncture. Where, the blue arrow is the puncture direction, The yellow area is the inner position of the puncture needle in the soft tissue (Recognition area after image processing). The red line is the horizontal line, The blue dotted line is the position of the needle axis.

puncture method and alternate rotation puncture method, and each puncture method was only performed once.

As shown in Figure 16, the internal image of the puncture needle in the tested soft tissue was observed, and the detected ultrasound image was processed by the medical image analysis method based on convolution neural network (CNN) [35]–[37]. The test results are shown in Figure 17.

During the test, the bevel of the needle tip of the puncture needle was facing upward (Its purpose is: in order to ensure the consistency of the image display process during the test, and facilitate the comparative analysis of its test results), the puncture time of of each method as 7s.

As can be seen from Figure 17(a₁) and 17(a₂), when the direct puncture method was used in the test, the puncture needle showed slight deflection in the lateral direction and large deflection in the longitudinal direction. It can be seen from Figure 17(b₁) and 17(b₂) that when the circumferential rotation puncture method was used in the test, the tissue in the area of the puncture needle is raised. This is because the circumferential rotation puncture method makes the puncture needle and the soft tissue to cause entanglement, and large deflection of the puncture needle in both the lateral and longitudinal directions. When the alternate rotation puncture

method was used in the experiment, it can be clearly seen from Figure 17(c₁) that the puncture needle is deflected in the tissue due to lateral drift and causes serious trauma to the soft tissue; However, it can be seen from Figure 17(c₂) that the deflection of puncture needle in the longitudinal direction has been significantly improved. It can be seen from Figure 17(d₁) and Figure 17(d₂) that when the sine rotation puncture method was used in the test, the deflection of the puncture needle in the soft tissue was better than the other three puncture methods, and the deflection problem had been greatly improved; But, there are still deflection angles δ_1 and δ_2 during the puncture process.

The performance comparison test verified the feasibility of the rotation puncture theory and the effectiveness of the sine rotation puncture method, and the test results were basically consistent with the theoretical analysis. However, to better apply the sine rotation puncture method to the radiotherapy of prostate cancer, it is necessary to analyze and optimize the variable parameters that affect the deflection of the puncture needle.

IV. PARAMETRIC ANALYSIS

According to the puncture requirements of prostate seed implantation, it was necessary to design a puncture control method that meets high precision, deep puncture and does not require fixation. Therefore, in the studied in the previous section, a control method based on sine rotation for soft tissue puncture was proposed, and the feasibility and effectiveness of this method for soft tissue puncture for prostate cancer had been verified through tests analysis. However, if this method is used for soft tissue puncture, there are still deflection angles of lateral and longitudinal between the needle and the soft tissue; Meanwhile, in the third section of the theoretical test and performance comparison test, it can be seen that it is not easy to select the control parameters that meet the best puncture effect according to the range of experience provided by the clinician. Therefore, for the control method based on sine rotation to puncture soft tissue, it was necessary to find out the control parameters that affect the puncture deflection, and conduct in-depth analysis and research on it.

Among the many parameters that affect the deflection of the puncture needle, it could be roughly divided into two categories according to variable parameters and invariable parameters; Among them, the invariable parameters include: the diameter, stiffness and tip angle of the puncture needle (The puncture needle for the implanted seed I125), puncture depth (Although the puncture depth can affect the deflection angle, it is necessary to implant the particles in the designated position during medical treatment) and soft tissue elastic modulus (The research object is mainly prostate soft tissue with cancer, and the elastic modulus of different patients is similar [34]). So, when analyzing the control parameters of the sine rotation puncture method, the analysis should be mainly based on the variable parameters, including: sine rotation frequency, puncture speed and rotation angle.

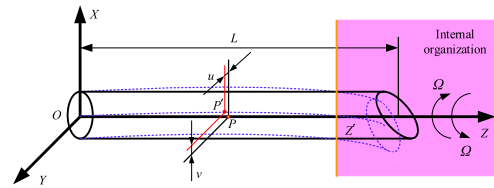


FIGURE 18. Euler beam model.

A. FREQUENCY INFLUENCE

When the doctor manipulates the robot to perform prostate soft tissue puncture by sine rotating needle control, due to the viscous damping inside the soft tissue, the deflection angle of the puncture needle can be effectively improved as the sine rotation frequency increases. However, when the puncture needle enters the internal soft tissue at a large rotation rate, it will generate modal vibration, which is easy to cause the deflection of the puncture needle. Therefore, an in-depth analysis of this situation is needed.

1) EULER BEAM MODEL

In the relevant research on puncturing soft tissue with sine rotation, the vibration of the puncture needle when it rotates at high speed can be expressed as the Euler beam model [38].

As shown in Figure 18, in the coordinate system $OXYZ$, the length of the puncture needle is L , and the mass per unit length is m ; Ω is the angular velocity of the puncture needle rotating around the Z axis (The magnitude and direction of Ω will change according to the sine rotation frequency); The black solid needle body is the initial position of the puncture needle, and it is set to have a point P on its central axis Z ; The blue dotted line is the deflection position of the puncture needle under the action of sine rotation; P' is a point on the central deflection axis Z' ; Therefore, in the XOY plane, the displacement of point P' relative to point P on the X axis and Y axis is represented by u and v respectively; The bending stiffness of the puncture needle in the XOZ plane and the YOZ plane can be expressed as EI .

According to the Bernoulli-Euler beam theory, the shear deformation and moment of inertia of the beam are very small and are ignored in the analysis. Then the total deformation of the puncture needle can be expressed as a vector r as:

$$r = ui + vj \tag{14}$$

where, i and j respectively represent unit vectors along the X -axis and Y -axis.

According to equation (14), the velocity of point P can be expressed as:

$$V = \dot{r} + \phi r = (\dot{u} - \Omega v)i + (\dot{v} + \Omega u)j \tag{15}$$

where, V represents the vibration speed of point P in the case of rotation; $\phi = \Omega k$, k is the unit vector in the Z -axis direction.

According to equation (15), the expressions of the kinetic energy T and the potential energy U of the Euler beam are:

$$\begin{cases} T = \frac{1}{2}m \int_0^L |v|^2 dz = \frac{1}{2}m \int_0^L \left[\left(\frac{du}{dt}\right)^2 + \left(\frac{dv}{dt}\right)^2 + 2\Omega\left(\frac{dv}{dt}u + \frac{du}{dt}v\right) + \Omega^2(u^2 + v^2) \right] dz \\ U = \frac{1}{2}EI \int_0^L \left(\frac{\partial^2 v}{\partial y^2}\right)^2 dz + \frac{1}{2}EI \int_0^L \left(\frac{\partial^2 u}{\partial x^2}\right)^2 dz \end{cases} \quad (16)$$

Applying Hamilton’s principle [38], it can be expressed in the form of Lagrange operator:

$$\tau \int_{t_1}^{t_2} (T - U + W)dt = 0 \quad (17)$$

When performing needle puncture, since the surface of the needle body exposed to the outside is not subjected to external force, the external force work W is set to 0; the Lagrangian coefficient $\tau = 1$. Equation (16) is substituted into equation (17), and perform integral processing to obtain the differential equation of vibration-deflection of the puncture needle during high-speed rotation:

$$\begin{cases} -m \frac{d^2 u}{dt^2} + m\Omega^2 u + 2m\Omega \frac{dv}{dt} - EI \frac{\partial^4 u}{\partial x^4} = 0 \\ -m \frac{d^2 v}{dt^2} + m\Omega^2 v - 2m\Omega \frac{du}{dt} - EI \frac{\partial^4 v}{\partial y^4} = 0 \end{cases} \quad (18)$$

2) LINE ART FIGURES

In the analysis of the sine rotation frequency, the Euler beam model is used to study the vibration-deflection problem of the puncture needle rotating and puncturing the soft tissue at high speed, and establish its vibration-deflection difference equation. According to equation (18) that since the fourth term had a fourth-order partial derivative, it is necessary to establish a difference equation to solve it [39]. According to the finite difference discretization method, the number of nodes of the puncture needle is set to N , then the length of each node is $h = L/N$, the boundary condition of the model is:

$$\begin{cases} u_0 = u'_0 = v_0 = v'_0 = 0 \\ u''_N = u'''_N = v''_N = v'''_N = 0 \end{cases} \quad (19)$$

where, u_0 and v_0 are the initial positions of the needle, and u_N and v_N are the end positions of the needle; Meanwhile, ‘’, ‘’, and ‘’ are the first, second, and third partial derivatives of u and v with respect to the X and Y directions, respectively.

First, the fourth derivative in the X and Y directions is difference processing. Since the boundary conditions in the X and Y directions are the same, the fourth derivative in the X direction is taken as an example for study. Then, according to the expanded form of Taylor’s formula, after using the second-order central difference, the general difference form of each derivative in the X direction can be obtained. Meanwhile, according to the difference equation [40] and boundary

conditions, it can be obtained as follows:

$$\begin{cases} u''''_1 = (7u_1 - 4u_2 + u_3)/h^4 \\ u''''_2 = (-4u_1 + 6u_2 - 4u_3 + u_4)/h^4 \\ u''''_n = (u_{n-2} - 4u_{n-1} + 6u_n - 4u_{n+1} + u_{n+2})/h^4 \\ u''''_{N-1} = (7u_{N-3} - 27u_{N-2} + 33u_{N-1} - 13u_N)/7h^4 \\ u''''_N = 12(u_{N-2} - 2u_{N-1} + u_N)/7h^4 \end{cases} \quad (20)$$

Meanwhile, the quality of each node can be expressed as $m \cdot h$ after difference, and according to equation (18), equation (19) and equation (20) the difference equation of the model is:

$$M\ddot{q} + C\dot{q} + Kq = 0 \quad (21)$$

where, M is the mass matrix of $(2N*2N)$, C is the structural damping matrix of $(2N*2N)$, K is the stiffness matrix of $(2N*2N)$, $q = [u_1, u_2, u_3, \dots, u_n; v_1, v_2, v_3, \dots, v_n]$.

3) SOLVE THE DIFFERENCE EQUATION

When the puncture robot uses high-frequency swing rotary puncture, combined with equation (21), and its the total displacement from point P to Point P' on the puncture needle in the X direction and the Y direction can be calculated:

$$\begin{cases} q(t) = Ae^{-\varepsilon\omega_n t} \sin(\omega_d t) \\ \varepsilon = C/2M\omega_n \\ \omega_d = \sqrt{1 - \varepsilon^2}\omega_n \\ \omega_n = \sqrt{K/M} \end{cases} \quad (22)$$

where, A (Amplitude) is a constant (It is related to the material properties of the puncture needle itself), $q(t)$ is the displacement of point P on axis Z , ε is the viscous damping ratio between the needle and the tissue ($\varepsilon < 1$), ω_d is the damped natural frequency, ω_n represents the undamped natural frequency.

When the puncture needle adopts sine rotation puncture, since equation (22) and equation (13) are basically the same, and the undetermined coefficient method can be used to correspond each of its coefficients one by one, its vibration deflection is proportional to the sine rotation frequency and amplitude. So, the higher the sine rotation frequency and the greater the rotation angle, the greater the vibration-deflection generated by the puncture, which seriously affects the puncture accuracy.

Combined with Figure 14(a), in order to avoid the puncture needle being friction adhered, entangled and wrapped by the soft tissue caused by the sine rotation frequency is too low (0Hz~0.12Hz). By continuing to test the circumferential friction force of the sine rotation puncture method (After the frequency is greater than 1 Hz), it can be known that when the rotation frequency exceeds 2.45 Hz, the circumferential friction force of the puncture needle in the soft tissue tends to be stable.

Therefore, the sine rotation frequency should be selected and optimized between 0.12Hz and 2.45 Hz.

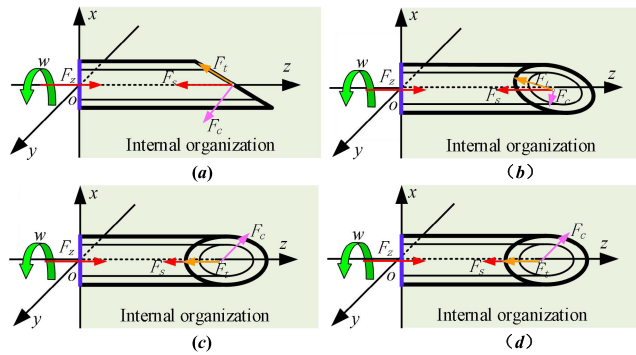


FIGURE 19. Rotation angle analysis. (a) Initial position, (b) $\alpha < 90^\circ$, (c) $\alpha = 90^\circ$, (d) $\alpha > 90^\circ$.

B. ROTATION ANGLE EFFECT

Through the analysis of the sine rotation frequency, it can be seen that when the sine rotation puncture soft tissue control method is used for puncture, the rotation angle of the puncture needle is too large, and the vibration deflection will be severe. However, if the rotation angle of the puncture needle is too small, it is easy to cause drift and deflect. The specific research analysis is shown in Figure 19. Where, w is the direction of rotation, and the puncture needle is inserted along the z -axis.

As the Figure 19 (a) shows that in addition to the puncture friction F_f , the shear force F_c of the puncture needle tip slope in the axial puncture resistance and the friction force F_t of the puncture needle tip slope can also affect the deflection of the puncture needle in the x -axis direction; At this time, the force of the puncture needle in the x -axis direction is the maximum, and the force in the y -axis direction is 0N.

As the Figure 19(b) shows the force analysis diagram (F_c and F_t) when the rotation angle α of the puncture needle is less than 90° . The force of the puncture needle in the x -axis direction will decrease, but the force component will start to produce the y -axis direction; So, when the rotation angle α of the puncture needle is less than 90° , it is easy to cause the needle tip to drift and deflect in the y -axis direction. As the Figure 19(c) is the forces analysis diagram when the puncture needle is rotated to 90° . The force of the puncture needle in the x -axis direction is 0, and the force in the y -axis direction reaches the maximum; So, when the puncture needle is rotated to 90° , it is easier to cause drift and deflect in the y -axis direction. As the Figure 19 (d) shows the force analysis diagram when the rotation angle α of the puncture needle is greater than 90° . The force direction of the puncture needle on the x -axis starts to increase in the opposite direction, which can compensate the deflection displacement of the puncture needle when the rotation angle is less than 90° .

When the w rotates in the reverse direction, the force in the x -axis direction is consistent with Figure 19, but the force in the y -axis direction is opposite.

According to the analysis of the circumferential friction test, when the rotation angle α is gradually increased to about

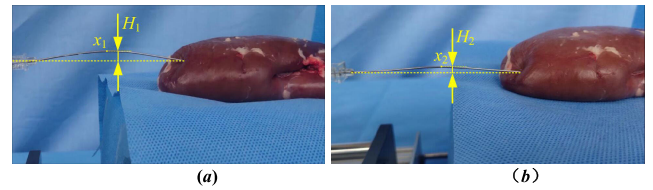


FIGURE 20. Puncture speed test. (a) Puncture speed is 1.1mm/s, (b) Puncture speed is 2.8mm/s.

390° under the condition of a sine rotation frequency of 0.12 Hz, the puncture needle body will slightly shake due to the rotation inertia of the servo motor B. So, considering the effect of the experiment, the sine rotation angle α should be optimized between 100° and 360° .

C. PUNCTURE SPEED EFFECT

When the puncture needle enters the soft tissue, due to its viscous damping effect, according to literature [24], [30], it could be known that the greater the puncture speed of the needle in the soft tissue, the greater the puncture friction between the needle and the soft tissue, thereby the easier it is to cause deflection. According to the analysis of the speed puncture test shows that if the puncture speed of the needle in the soft tissue is too low, it will cause the puncture needle to squeeze the surface of the soft tissue and cause the needle shaft to bend. The test result is shown in Figure 20. Where, x_1 and x_2 are the highest point of the bend of the needle body; The yellow dotted line is the horizontal position of the puncture needle; H_1 and H_2 as the bending displacement of the puncture needle body.

According to Figure 20(a), when the puncture depth as 5mm and the needle puncture speed as 1.1mm/s, the total kinetic energy of the puncture mechanism is small, so that the needle body does not have enough inertial force to break through the elastic tension on the surface of the soft group; This will cause the puncture needle to bend, and the needle tip will not be able to penetrate the soft tissue surface. By observing the result in Figure 20(b), when the puncture depth as 5mm and the puncture speed as 2.8mm/s, the puncture needle just penetrate the soft tissue due to the increase of the total kinetic energy of the puncture mechanism; But, its internal tissue still forms a large resistance to the puncture needle and bends, and the corresponding H_2 at point x_2 on the needle shaft is smaller than the corresponding H_1 at point x_1 , the puncture performance is significantly improved. Under the conditions of the above two puncture speeds, if you continue to increase the puncture depth, the soft tissue will drift and deflect.

In the experiment, it is necessary to consider the inevitable transmission and debugging errors of the entire puncture test system. In order to ensure the test effect, the puncture speed is selected to be optimized between 5mm/s and 45 mm/s. Where, 5mm/s is the minimum puncture speed of the soft tissue without drift measured in the experiment, and 45mm/s is the maximum puncture speed of the robot itself.

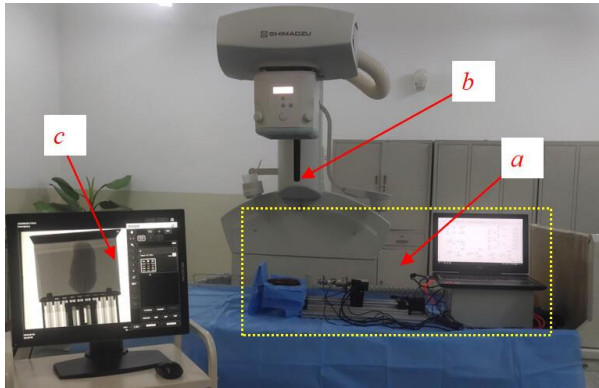


FIGURE 21. Optimal experiment system of sine rotation puncture parameters.

V. PARAMETER OPTIMIZATION EXPERIMENT

Through the analysis of the variable parameters of the sine rotation puncture method, their optimal area is determined. Therefore, in order to ensure the accuracy of the sine rotation soft tissue puncture control method and improve the therapeutic effect of the prostate puncture seed implantation surgery, in the follow-up research, it is necessary to further optimize its three variable parameters.

In addition, among all kinds of parameters optimization methods, Particle Swarm Optimization (PSO) algorithm [41]–[43], Genetic Algorithm (GA) [44]–[46], and in recent years, Cheng *et al.* [47], [48] newly proposed methods such as Global/local Linked Driven Optimization Strategy (GLDOS) and Improved Decomposed-Coordinated Kriging Modeling Strategy (IDCKMS) are representative. The above optimization methods can efficiently and accurately optimize and solve specific objective function models; However, for problems that need to first construct an optimized objective function model through experiments, and then optimize its parameters (Such as this paper will optimize the control parameters of sine rotating puncture, which belongs to this kind of optimization problem), the experimental statistical analysis method is generally used for optimization analysis.

A. EXPERIMENT PREPARATION AND METHOD

1) TEST PREPARATION

a: EXPERIMENT SITE

The experiment site of the sine rotation puncture parameter optimization experiment as Department of Imaging, The People's Hospital of Hailun, Suihua City, Heilongjiang Province, China.

b: EXPERIMENT EQUIPMENT

Figure 21 shows the experiment system with optimized parameters. Where, the icon *a* is the test platform of acupuncture prostate soft tissue, the icon *b* is a 3D X-ray scanner manufactured by SHIMADZU, Japan (It is mainly used to scan and observe the deflection angle of the puncture needle in the soft tissue under test), the icon *c* is an X-ray

TABLE 2. Experimental factors level coding table.

Coding value	Experimental factors		
	Rotation frequency x_1 (Hz)	Rotation angle x_2 (°)	Puncture speed x_3 (mm/s)
High asterisk arm (+1.682)	2.45	360.0	45
High level (+1)	0.60	152.7	37
Zero level (0)	1.30	230.0	25
Low level (-1)	2.00	307.3	13
Low asterisk arm (-1.682)	0.12	100.0	5
Level spacing	0.70	77.3	12

display used to observe and collect internal images of soft tissues.

2) TEST METHOD

① The optimization test of the parameters of the sine rotation puncture is a multi-objective optimization test, it is generally optimized using a full factor test method, but this will lead to too large number of trials and large errors in data results. So, this article is based on the optimization range of the sine rotation puncture parameters, the experiment was designed by the quadratic regression orthogonal rotation combination theory of three factors and five levels [49]–[51].

This method combines the advantages of orthogonal analysis and regression analysis, it has the characteristics of flexible testing, simple calculation, and avoiding correlation interference between various parameters [52]. Meanwhile, this method not only guarantees to provide abundant information for the test, but also reduces the number of tests, and it can replace full experiment [52]. In addition, this method can also help the tester to directly compare the good and bad of the predicted value during the experiment, from which it is easy to find the relatively good experimental parameter area [53].

Therefore, combine the experimental tasks to draw a factor level coding table of three factors and five levels, and select the level values of each factor and level spacing according to literature [52]–[54], the level coding table of the experimental factors is shown in Table 2.

② For soft tissue experiments, pig kidney was still selected and placed freely on the soft tissue placement stent. The puncture depth as 80mm. The puncture needle was a medical surgical semi-flexible seed implant needle (The starting position of the bevel of the needle tip was upward in the positive direction). The selection of the experimental indexes could reflect the deflection angles of puncture accuracy (lateral deflection angle, and longitudinal deflection angle). As shown in Figure 22, it was an X-ray scan image (image obtained by precise processing through an image recognition method based on literatures [55]–[59]). Where, The yellow-green border represents the image recognition area, and the red line represents the horizontal line.

As the Figure 22 clearly shows the deflection Angle of the puncture needle inside the soft tissue for easy observation.

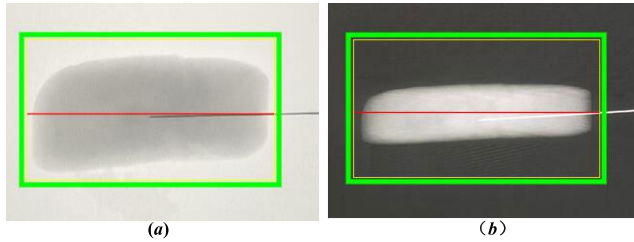


FIGURE 22. The X-ray scan image after algorithm processing. (a) The vertical view of the X-ray through perspective (Observe the lateral deflection angle), (b) The side view of the X-ray through radiography (Observe the longitudinal deflection angle).

TABLE 3. Experimental scheme and results.

No.	Rotation frequency x_1 (Hz)	Rotation angle x_2 (°)	Puncture speed x_3 (mm/s)	Lateral deflection angle Y_1 (°)	Longitudinal deflection angle Y_2 (°)
1	0.60	152.7	13	1.40	1.93
2	2.00	152.7	13	1.52	1.85
3	0.60	307.3	13	1.92	1.71
4	2.00	307.3	13	1.96	1.68
5	0.60	152.7	37	2.16	2.29
6	2.00	152.7	37	2.01	2.13
7	0.60	307.3	37	1.78	2.25
8	2.00	307.3	37	1.61	2.19
9	0.12	230.0	25	1.88	2.05
10	2.45	230.0	25	1.71	1.94
11	1.30	100.0	25	1.83	2.07
12	1.30	360.0	25	2.02	2.00
13	1.30	230.0	5	1.67	1.63
14	1.30	230.0	45	1.75	2.32
15	1.30	230.0	25	1.38	1.79
16	1.30	230.0	25	1.41	1.81
17	1.30	230.0	25	1.43	1.82

At the same time, during the measurement of data, the identified image data was calculated according to equation (3) and equation (7), and its deflection angle is obtained and recorded.

③ According to the level coding table of experimental factors, the Response Surface/Central Composite module in the Design-Expert 8.0.6 software was used to design the quadratic regression orthogonal combination experimental scheme, a total of 17 groups of experiments were conducted. To ensure the generality and universality of experimental results, prevent excessive deviation in a single experiment, each group of experiments was repeated 5 times, remove one highest value and one lowest value, take the average, and the obtained average values of the lateral deflection angle and the longitudinal deflection angle were filled in the corresponding to experimental groups. Where, the deflection angle in each direction took absolute value. The experimental scheme and results are shown in Table 3.

B. RESULTS ANALYSIS

Used the efficient hybrid method of the RSM and the LAPO algorithm for multi-objective optimization design in Design-Expert 8.0.6 software to perform quadratic regression analysis on the above experimental results, and performed multiple regression fitting to obtain regression equations for

two experimental indexes, including lateral deflection angle Y_1 and longitudinal deflection angle Y_2 . At the same time, the variance was calculated significance tests.

1) DEFLECTION ANGLE REGRESSION ANALYSIS

Through the LAPO algorithm performed multiple regression fitting on the experimental data in Table 3, and performed variance analysis on the fitting equation, the variance analysis results of the lateral deflection angle Y_1 and the longitudinal deflection angle Y_2 are obtained, as shown in Table 4. As can be seen from Table 4, for the lateral deflection angle and the longitudinal deflection angle, and combined with the P value result after F test, the primary and secondary order of the interaction between factors and factors as: $(x_2x_3, x_2^2) > x_1^2 > x_3^2 > x_3 > x_1x_3 > x_2 > x_1 > x_1x_2$ and $(x_3, x_1^2, x_2^2, x_3^2) > (x_1, x_2x_3) > x_2 > x_1x_2 > x_1x_3$. At the same time, the models of the overall tests are extremely significant, and the test results of the lack of fit are not significant (When $P > 0.1$, it is not significant; Among them, the lateral deflection angle: $P = 0.1157$ and the longitudinal deflection angle: $P = 0.2777$), indicating that the experimental results are correct and valid. Therefore, this article took the three parameters (Rotation frequency, rotation angle and puncture speed) of the sine rotation continuous puncture control method as the test factors and the deflection angles of the lateral and the longitudinal as the test indicators, and combined with the quadratic regression orthogonal rotation combination theory of three factors and five levels to establish the experimental models, and the models have practical analytical significance for improving its puncture performance.

After removing the insignificant term x_1x_2 in the lateral deflection angle and the insignificant term x_1x_3 in the longitudinal deflection angle, analyzed the variance again to obtain the regression equation of the influence of each factor on the lateral and longitudinal deflection angle:

$$Y_1 = 1.41 - 0.036x_1 + 0.037x_2 + 0.067x_3 - 0.059x_1x_3 - 0.22x_2x_3 + 0.13x_1^2 + 0.17x_2^2 + 0.097x_3^2 \quad (23)$$

$$Y_2 = 1.81 - 0.039x_1 - 0.036x_2 + 0.21x_3 + 0.019x_1x_2 + 0.051x_2x_3 + 0.063x_1^2 + 0.078x_2^2 + 0.057x_3^2 \quad (24)$$

where, x_1 , x_2 , and x_3 represent the coding values of rotation frequency, rotation angle and puncture speed; Y_1 and Y_2 represent the coding values of the experimental indexes (Lateral deflection angle and longitudinal deflection angle).

Through the study of regression equations (23) and (24), it could be seen that the influencing factors (Rotation frequency x_1 , rotation angle x_2 and needle advancement speed x_3) of the sine rotation puncture method affect the lateral deflection angle (Y_1) and longitudinal deflection angle (Y_2) have a significant impact.

In addition, the optimal parameters can also be predicted and solved according to the above regression equation.

TABLE 4. Variance analysis of lateral deflection angle and longitudinal deflection angle.

Items	Variation source	Sum of squares		Degrees of freedom		Mean square		F value		P value	
		Data 1	Data 2	Data 1	Data 2	Data 1	Data 2	Data 1	Data 2	Data 1	Data 2
Lateral deflection angle	Model	0.93	0.93	9	8	0.1	0.12	23.83	29.38	0.0002***	<0.0001***
	x_1	0.018	0.018	1	1	0.018	0.018	4.07	4.47	0.0834*	0.0674*
	x_2	0.019	0.018	1	1	0.019	0.018	4.28	4.64	0.0773*	0.0635*
	x_3	0.061	0.061	1	1	0.061	0.061	14.13	15.51	0.0071***	0.0043***
	x_1x_2	0.0012	—	1	—	0.0012	—	0.29	—	0.6076	—
	x_1x_3	0.029	0.029	1	1	0.029	0.029	6.66	7.31	0.0365**	0.0269**
	x_2x_3	0.38	0.038	1	1	0.38	0.038	87.48	96.01	<0.0001***	<0.0001***
	x_1^2	0.19	0.19	1	1	0.19	0.19	42.79	46.96	0.0003***	0.0001***
	x_2^2	0.34	0.34	1	1	0.34	0.34	78.86	86.55	<0.0001***	<0.0001***
	x_3^2	0.11	0.11	1	1	0.11	0.11	24.96	27.4	0.0016***	0.0008***
	Residual	0.03	0.032	7	8	0.004	0.004	—	—	—	—
Lake of Fit	0.029	0.03	5	6	0.006	0.005	9.16	7.96	0.1013	0.1157	
Cor Total	0.96	0.96	16	16	—	—	—	—	—	—	
Longitudinal deflection angle	Model	0.76	0.75	9	8	0.084	0.094	153.64	141.27	<0.0001***	<0.0001***
	x_1	0.021	0.021	1	1	0.021	0.021	38.76	31.74	0.0004***	0.0005***
	x_2	0.018	0.018	1	1	0.018	0.018	32.58	26.68	0.0007***	0.0009***
	x_3	0.6	0.6	1	1	0.6	0.6	1091.31	891.92	<0.0001***	<0.0001***
	x_1x_2	0.0028	0.0028	1	1	0.0028	0.0028	5.15	4.22	0.0576*	0.0741*
	x_1x_3	0.0015	—	1	—	0.0015	—	2.77	—	0.1401	—
	x_2x_3	0.021	0.021	1	1	0.021	0.021	38.46	31.5	0.0004***	0.0005***
	x_1^2	0.046	0.046	1	1	0.046	0.046	84.1	68.87	<0.0001***	<0.0001***
	x_2^2	0.069	0.069	1	1	0.069	0.069	126.26	103.4	<0.0001***	<0.0001***
	x_3^2	0.037	0.037	1	1	0.037	0.037	67.23	55.06	<0.0001***	<0.0001***
	Residual	0.0038	0.0053	7	8	0.0005	0.0007	—	—	—	—
Lake of Fit	0.0033	0.0049	5	6	0.0007	0.0008	2.88	3.48	0.2777	0.2777	
Cor Total	0.76	0.76	16	16	—	—	—	—	—	—	

Data1 is the original data, Data2 is the data after removing insignificant factors; “—” means no data.

“***” means extremely significant ($P < 0.01$), “**” means very significant ($0.01 \leq P < 0.05$), “*” means significant ($0.05 \leq P < 0.1$).

2) RESPONSE SURFACE ANALYSIS

The data of the sine rotation puncture experiments was processed by the RSM-based response surface analysis module in the Design-Expert 8.0.6 software to obtain the response surface of the influencing factors x_1 , x_2 , and x_3 to the experimental indexes Y_1 and Y_2 , as shown in Figure 23. Where, “0” represents the factor coding value corresponding to the factor’s level value. In the analysis of response surface, the value of 0 level is generally taken.

It can be seen from Figure 22 (a_1) that when the rotation frequency is constant, the lateral deflection angle first decreases and then increases with the increase of puncture speed. The reason is that as the puncture speed increases, the puncture needle can better overcome the surface tension and internal resistance of the soft tissue, and reduce the lateral offset caused by the extrusion deformation during puncture; When the puncture speed continues to increase, the friction force on the puncture needle body and the shear force of the needle tip bevel also continue to increase, which in turn causes the lateral deviation of the puncture needle to increase. When the puncture speed is constant, the lateral deflection angle first decreases and then increases with the increase of the rotation frequency. The reason for the analysis is that with the increase of the rotation frequency, the puncture needle can well overcome the offset caused by the adhesion and package

of the soft tissue; When the rotation frequency continues to increase, the offset of the puncture needle also increases, which is consistent with the previous theoretical.

It can be seen from Figure 23 (a_2) that when the rotation angle is the smaller, the lateral deflection angle increases with the increase of the puncture speed, which is consistent with the previous theoretical analysis. When the rotation angle is the larger, the lateral deflection angle decreases with the increase of puncture speed; The reason is that as the rotation angle increases, the puncture needle offset increases. If the puncture speed increases, the puncture needle can quickly reach the designated position before the offset caused by the increase in the rotation angle is not obvious enough. When the puncture speed is the smaller, the lateral deflection angle increases with the increase of the rotation angle, which shows that the lateral deflection angle is significantly affected by the rotation angle at this time, and is consistent with the theoretical analysis; At the same time, when the puncture speed is the higher, the lateral deflection angle decreases with the increase of the rotation angle, which means that when the circumferential friction of the puncture needle gradually increases, its axial puncture resistance will decrease, thereby inhibiting offset of the puncture needle.

In the same way, the response surface of the longitudinal deflection angle shown in Figure 23 (b_1) and Figure 23 (b_2) is

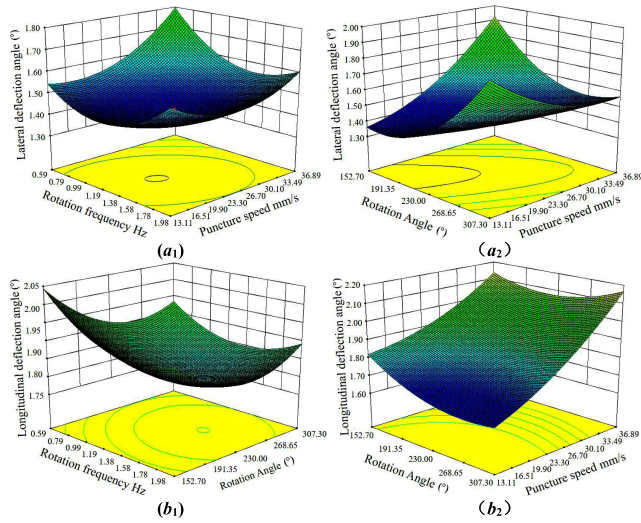


FIGURE 23. Two-factor response surface of deflection angle of the lateral and longitudinal. (a₁) $Y_1(x_1, 0, x_3)$, (a₂) $Y_1(0, x_2, x_3)$, (b₁) $Y_2(x_1, x_2, 0)$, (b₂) $Y_2(0, x_2, x_3)$.

consistent with Figure 23 (a₁), Figure 23 (a₂) and theoretical analysis. However, a comparative analysis of Figure 23 (b₂) and Figure 23 (a₂) shows that when the initial circumferential position of the puncture needle is the positive direction of the needle tip bevel facing upward, as the angle of rotation increases, the needle tip bevel receives a lateral component force is the greater than a longitudinal component force.

Therefore, in the experiment, although the different initial circumferential positions of the puncture needle will cause the deviation angle response surface to be different, but the overall deflection angle of the puncture needle and the influence law of various factors remain unchanged. So, the initial circumferential position of the puncture needle has no influence on the test analysis and test results.

C. PARAMETER OPTIMIZATION

In the puncture test, the purpose of parameter optimization of the sine rotation puncture method is to obtain the optimal parameter combination when puncturing the target point of the lesion, to minimize the offset and the deflection of the puncture needle during the puncture of the soft tissue of the prostate, thereby improve the puncture accuracy, and ensure treatment effect. Through the analysis of the deflection angle two-factor response surface in Figure 23, and used the optimization module in Design-Expert 8.0.6 software to solve the regression models of equation (23) and equation (24). Meanwhile, according to the actual working conditions of the prostate seed implantation surgery and the analysis results of the response surface, the optimization constraint conditions for the selected experimental factors are:

$$f_{Target} = \{ \min Y_1(x_1, x_2, x_3); \min Y_2(x_1, x_2, x_3) \} \quad (25)$$

$$f_{Constraint} = \begin{cases} a_1 \leq x_1 \leq a_2 \\ b_1 \leq x_2 \leq b_2 \\ c_1 \leq x_3 \leq c_2 \end{cases} \quad (26)$$

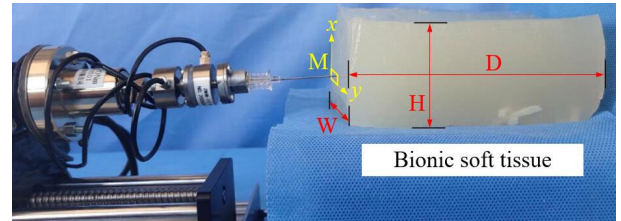


FIGURE 24. Soft tissue puncture comparative test.

where, f_{Target} is the optimization objective function, $f_{Constraint}$ is the factor constraint function; $a_1 = 0.6\text{Hz}$, $a_2 = 2\text{Hz}$, $b_1 = 152^\circ$, $b_2 = 307^\circ$, $c_1 = 10\text{mm/s}$, $c_2 = 30\text{mm/s}$:

Through equation (23), equation (24), equation(25), and equation (26), the parameters were optimized and solved, and the optimal parameters of the sine rotation puncture control method were obtained: the rotation frequency was 1.32Hz, and the rotation angle was 202.88°, the puncture speed was 12.25mm/s;

At this time, the optimal parameter was substituted into the regression equation to calculate, when the puncture needle penetrates the soft tissue, the theoretical lateral deflection angle is 1.38°, and the theoretical longitudinal deflection angle is 1.65°.

VI. COMPARISON VERIFICATION TESTS

In order to verify the rationality of the sine rotary puncture soft tissue control method and the reliability of the optimal parameters, this paper used the control method comparison test and the parameter performance comparison test for analysis. Where, the rotation frequency, rotation angle and puncture speed of the sine rotation puncture method adopts 1.32Hz, 202.88° and 12.25mm.

A. CONTROL METHOD COMPARISON TEST

In order to verify the rationality of the sine rotation puncture soft tissue control method, sine rotating puncture method was compared with the puncture methods such as direct puncture, high-speed vibration-rotation [30] and alternating rotation duty cycle [26].

1) TEST TARGET

A bionic PVA hydrogel with mechanical properties similar to human soft tissue was prepared as the puncture test target [60], as shown in Figure 24. Where, the longitudinal section width W of the test target is 120 mm, the height H is 120 mm, and the longitudinal length (depth) D is 200 mm.

2) TEST DEVICE

The test device shown in Figure 24 is consistent with the test platform shown in Figure 3. But, the high-speed vibration-rotation puncture needle penetration test used the test device shown in literature [30].

③ Testing method: The first, marked the initial point of puncture at the front and back of the longitudinal section of the test target, and serve as the origin of the coordinate.

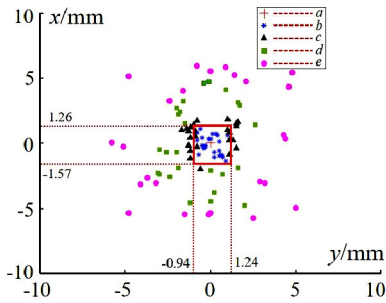


FIGURE 25. Control method comparison test result (The red frame is the concentrated area of the sine rotation puncture method in 25 punctures). Where, *a* is the target position, *b* is the sine rotation puncture method, *c* is the alternate rotation puncture method, *d* is the circumferential rotation puncture method, *e* is the direct puncture method.

The second, puncture was conducted by using the above four puncture methods, and coordinate paper (1mm cell) was used to mark the position of the needle protruding from the back of the measured soft tissue section; The finally, each method was performed 25 times, and the data results are recorded.

3) TEST RESULTS

The recorded data results were processed and analyzed by Matlab2016a software, as shown in Figure 25 (The coordinate system range is the yellow area M on the *xy* plane in Figure 24).

According to the statistical literature [61]–[64], it can be seen that when puncturing the bionic PVA hydrogel, the puncture accuracy of the existing particle implantation robot is generally (0.3mm~3mm). Therefore, it can be seen from Figure 25 that, except for direct puncture, all other puncture methods meet the accuracy requirements, but in the area of the sine rotation puncture method, the longitudinal *x* is (−1.27mm~1.26mm) and the lateral *y* is (−0.94mm~1.24mm), the puncture point is less than 0.3mm, which accounts for about 12% of the total points. Compared with other puncture control methods, it has the best performance and simple operation. The test results verify the rationality of the sine rotation puncture control method.

B. PARAMETET PERFORMANCE COMPARISON TEST

In order to verify the reliability of using the quadratic regression orthogonal rotation combination test method to optimize the parameters, the optimal parameter combination of the sine rotation puncture method was compared with other combination parameters in the range.

① Test target: The pig kidney.

② Test instrument: The test platform shown in Figure 3; A 3D X-ray scanner manufactured by SHIMADZU, Japan.

③ Testing method: (1). In order to ensure the effectiveness of the control method comparison test, the level combination of its parameters needs to be reselected. Its principles were:

First, the new level value had to be within the original optimization interval.

TABLE 5. New orthogonal combination and comparison test results.

No.	Test factors			Impact indicators	
	X_1 (Hz)	X_2 (°)	X_3 (mm/s)	γ_1 (°)	γ_2 (°)
1	0.50	120.00	5.65	1.71	1.89
2	0.50	180.00	11.25	1.63	1.81
3	0.50	240.00	16.88	1.87	2.02
4	1.25	120.00	11.25	1.59	1.82
5	1.25	180.00	16.88	1.65	1.85
6	1.25	240.00	5.62	1.62	1.91
7	2.00	120.00	16.88	1.68	2.05
8	2.00	180.00	5.62	1.57	1.83
9	2.00	240.00	11.25	1.73	1.82
10	1.32	202.88	12.25	1.36	1.61
11	1.32	202.88	12.25	1.32	1.59
12	1.32	202.88	12.25	1.33	1.63

X_1 is the rotation frequency, X_2 is the rotation angle, X_3 is the puncture speed; γ_1 is the lateral deflection angle, γ_2 is the longitudinal deflection angle.

Groups 1 to 9 are the reference group; Groups 10 to 12 are the verification group.

Second, the new level interval had to contain the optimal parameter value.

Third, the new level combination was different from the level combination of the quadratic regression orthogonal rotation combination test.

Last, the new level combination could represent the whole combination.

(2) Based on the theoretical test parameter values in Section 3 and the optimal parameter values in Section 5, the $L_9(3^4)$ orthogonal test method was applied to group the optimized ranges of its rotation frequency, rotation angle and puncture speed [65], [66].

(3) According to the orthogonal horizontal combination, the puncture test was shown in Table 5, and the process was the same as that in Section 5.

④ Test Results: As shown in Table 5, through the analysis and comparative of the reference group and the verification group, it can be seen that the sine rotation puncture soft tissue control method adopts the optimal control parameters, and its puncture effect is significantly better than other control parameters. Meanwhile, the test indicators obtained by the verification group test are basically consistent with the theoretical test results calculated by the regression equation, which proves the accuracy of the regression equations (23) and (24) and the effectiveness of the optimal parameters.

X_1 is the rotation frequency, X_2 is the rotation angle, X_3 is the puncture speed; γ_1 is the lateral deflection angle, γ_2 is the longitudinal deflection angle.

Groups 1 to 9 are the reference group; Groups 10 to 12 are the verification group.

So, the results of the parameter performance comparison test verify the reliability of using the quadratic regression orthogonal rotation combined test analysis method to optimize the parameters of the sine rotation puncture method.

VII. CONCLUSION

The research object of this article is the puncture control method of the prostate seed implantation robot. In the actual operation, due to the complex forces between the puncture

needle and the soft tissue causes its deflection, which reduces the puncture accuracy and affects the therapeutic effect of the seed implantation. Therefore, this article mainly studies this problem, through the force balance analysis of the soft tissue acupuncture process, it was found that the large puncture friction between the needle body and the soft tissue is the main reason for the large deflection of the puncture needle, which affects the accuracy of puncture positioning.

On this basis, through the theoretical analysis of rotating puncture, it can be known that increasing the circumferential friction of the puncture needle can reduce the axial puncture friction. Therefore, in this paper, a sine rotation continuous puncture control method is proposed. Combined with the existing puncture methods for comparative analysis, theoretical tests and performance tests have proved its feasibility and effectiveness, which can effectively improve its puncture accuracy. At the same time, combined with the theoretical research on the control parameters of the sine rotation puncture, the rotation frequency, the rotation angle and the puncture speed were selected as the experimental factors, and the lateral and the longitudinal deflection angles were selected as the experimental indicators, and the three-factor and five-level quadratic regression orthogonal combination design theory was adopted to optimize its control parameters. Through the comparative verification test, the rationality of the control method of the sine rotation continuous puncture and the reliability of the optimal parameters were verified, which effectively improved the puncture accuracy; At the same time, the accuracy of the regression models is also verified.

According to shear wave elastography technology, real-time tissue elastography ultrasound diagnostic equipment was used to measure the elastic modulus of the kidneys of many large mammals. It was found that the elastic modulus of pig kidney is the closest to that of human prostate with cancer, which can be a good substitute for prostate cancer patients for experimental research.

In the puncture test, although the sine rotating puncture method with optimized parameters could greatly improve the deflection of the puncture needle, the slight deflection caused by the immutable parameters of the medical puncture itself still exists. Therefore, in the future research work, it is necessary to conduct in-depth research and improvement on the material properties, structural shape and size parameters of medical puncture needles.

The research work in this paper provides reference for the control research on improving the positioning accuracy of minimally invasive puncture operation (Including: design or improvement of puncture control methods and puncture of other soft tissue organs of the human body, etc).

ACKNOWLEDGMENT

Bing Li would like to thank Prof. Cao Liying and the Department of Medical Imaging from Hailun People's Hospital, Suihua City, Heilongjiang Province, China, for their support and help in the tests.

REFERENCES

- [1] Y. Zhang, Y. Liang, X. Wang, and Y. Xu, "Design and experimental study of joint torque balance mechanism of seed implantation articulated robot," *Adv. Mech. Eng.*, vol. 7, no. 6, pp. 1–10, Mar. 2015.
- [2] A. Liao, J. Wang, J. Wang, H. Zhuang, and Y. Zhao, "Relative biological effectiveness and cell-killing efficacy of continuous low-dose-rate 125I seeds on prostate carcinoma cells *in vitro*," *Integrative Cancer Therapies*, vol. 9, no. 1, pp. 59–65, Feb. 2010.
- [3] R. L. Siegel, K. D. Miller, and A. Jemal, "Cancer statistics, 2018," *CA A, Cancer J. Clinicians*, vol. 68, no. 1, pp. 7–30, Jan. 2018.
- [4] C. E. DeSantis, K. D. Miller, A. Goding Sauer, A. Jemal, and R. L. Siegel, "Cancer statistics for African Americans, 2019," *CA A, Cancer J. Clinicians*, vol. 69, no. 3, pp. 211–233, May 2019.
- [5] R. Siegel, K. Miller, and A. Jemal, "Cancer statistics, 2020," *Ca-A Cancer J. Clinicians*, vol. 70, no. 1, pp. 7–30, 2020.
- [6] J. Jiang, Z. Huang, X. Guo, Y. Zhang, and Y. Xu, "Study on the design and experiment of RCM for transrectal ultrasound probe position and posture adjustment," *Chinese J. Sci. Instrum.*, vol. 40, no. 2, pp. 164–173, 2019, doi: 10.19650/j.cnki.cjsi.J1804027.
- [7] Y. Zhu, S. J. Freedland, and D. Ye, "Prostate cancer and prostatic diseases best of Asia, 2019: Challenges and opportunities," *Prostate Cancer Prostatic Diseases*, vol. 23, no. 2, pp. 197–198, Jun. 2020.
- [8] R. Chen, D. Sjoberg, Y. Huang, L. Xie, L. Zhou, D. He, A. Vickers, and Y. Sun, "Prostate specific antigen and prostate cancer in Chinese men undergoing initial prostate biopsies compared with Western cohorts," *J. Urol.*, vol. 197, no. 1, pp. 90–96, Jan. 2017.
- [9] L. Zhuo, Y. Cheng, Y. Pan, J. Zong, W. Sun, L. Xu, M. Soriano, Y. Song, J. Lu, and S. Zhan, "Prostate cancer with bone metastasis in Beijing: An observational study of prevalence, hospital visits and treatment costs using data from an administrative claims database," *BMJ Open*, vol. 9, no. 6, pp. 1–8, Jun. 2019.
- [10] X. Zhu, A. Zheng, Z. Wang, and Q. Shao, "Prostate cancer prevention trial risk calculator for evaluating the risk of prostate cancer in the high-risk Chinese population," *Zhonghua Nan Ke Xue Nat. J. Ofandrol*, vol. 24, no. 2, pp. 142–146, Feb. 2018.
- [11] R. Chen, L. Xie, W. Xue, Z. Ye, L. Ma, X. Gao, S. Ren, F. Wang, L. Zhao, C. Xu, and Y. Sun, "Development and external multicenter Validation of Chinese prostate cancer consortium prostate cancer risk calculator for initial prostate biopsy," *Urol. Oncol., Seminars Original Invest.*, vol. 34, no. 9, pp. 416.e1–416.e7, Sep. 2016.
- [12] D. Ye, W. Zhang, L. Ma, C. Du, L. Xie, Y. Huang, Q. Wei, Z. Ye, and Y. Na, "Adjuvant hormone therapy after radical prostatectomy in high-risk localized and locally advanced prostate cancer: First multicenter, observational study in China," *Chin. J. Cancer Res.*, vol. 31, no. 3, pp. 511–520, Mar. 2019.
- [13] J. Lin, X. Yu, J. Ji, X. Yang, J. Jin, L. Liu, J. Su, Y. Li, and M. Shang, "High incidence of incidental prostate cancer in transurethral resection of prostate specimens in China. The value of pathologic review," *Anal. Quantum Cytopathol. Histopathol.*, vol. 38, no. 1, pp. 31–37, Feb. 2016.
- [14] B. Li, Y. Zhang, L. Yuan, and X. Xi, "Study on the low velocity stability of a prostate seed implantation Robot's rotatory joint," *Electronics*, vol. 9, no. 2, p. 284, Feb. 2020.
- [15] Y. Liang, D. Xu, B. Wang, Y. Zhang, and Y. Xu, "Experimental study of needle insertion strategies of seed implantation articulated robot," *J. Mech. Med. Biol.*, vol. 18, no. 3, May 2018, Art. no. 1850023.
- [16] T. K. Podder, I. Buzurovic, K. Huang, T. Showalter, A. P. Dicker, and Y. Yu, "Reliability of EUCLIDIAN: An autonomous robotic system for image-guided prostate brachytherapy," *Med. Phys.*, vol. 38, no. 1, pp. 96–106, Jan. 2011.
- [17] H. Su, W. Shang, G. Cole, G. Li, K. Harrington, A. Camilo, J. Tokuda, C. M. Tempny, N. Hata, and G. S. Fischer, "Piezoelectrically actuated robotic system for MRI-guided prostate percutaneous therapy," *IEEE/ASME Trans. Mechatronics*, vol. 20, no. 4, pp. 1920–1932, Aug. 2015, doi: 10.1109/TMECH.2014.2359413.
- [18] S. Russo, P. Dario, and A. Menciassi, "A novel robotic platform for laser-assisted transurethral surgery of the prostate," *IEEE Trans. Biomed. Eng.*, vol. 62, no. 2, pp. 489–500, Feb. 2015, doi: 10.1109/TBME.2014.2358711.
- [19] L. Chen, T. Paetz, V. Dicken, S. Krass, J. A. Issawi, D. Ojdanic, S. Krass, G. Tigelaar, J. Sabisch, A. V. Poelgeest, and J. Schaechtele, "Design of a dedicated five degree-of-freedom magnetic resonance imaging compatible robot for image guided prostate biopsy," *J. Med. Devices*, vol. 9, no. 1, Mar. 2015, Art. no. 015002.

- [20] S. Elayaperumal, M. R. Cutkosky, P. Renaud, and B. L. Daniel, "A passive parallel master-slave mechanism for magnetic resonance imaging-guided interventions," *J. Med. Devices*, vol. 9, no. 1, Mar. 2015, Art. no. 011008.
- [21] Y. Fu and B. Pan, "Research progress of surgical robot for minimally invasive surgery," *J. Harbin Inst. Technol.*, vol. 51, no. 1, pp. 1–15, Jan. 2019, doi: 10.11918/j.issn.0367-6234.201806178.
- [22] Y. Zhang, J. Peng, and L. Gang, "Research on the segmentation method of prostate magnetic resonance image based on level set," *Chin. J. Sci. Instrum.*, vol. 38, no. 2, pp. 416–424, Feb. 2017, doi: 10.19650/j.cnki.cjsi.2017.02.020.
- [23] R. Seifabadi, N. B. J. Cho, S.-E. Song, J. Tokuda, N. Hata, C. M. Tempny, G. Fichtinger, and I. Lordachita, "Accuracy study of a robotic system for MRI-guided prostate needle placement," *Int. J. Med. Robot. Comput. Assist. Surgery*, vol. 9, no. 3, pp. 305–316, Sep. 2013, doi: 10.1002/rcs.1440.
- [24] Y. Liang, "Research on key technology of radioactive seed implantation robot for prostate," Ph.D. dissertation, Dept. Mechatronics Eng., Harbin Univ. Sci. Technol., Harbin, China, 2017.
- [25] D. S. Minhas, J. A. Engh, M. M. Fenske, and C. N. Riviere, "Modeling of needle steering via duty-cycled spinning," in *Proc. 29th Annu. Int. Conf. IEEE Eng. Med. Biol. Soc.*, Aug. 2007, pp. 2756–2759, doi: 10.1109/IEMBS.2007.4352899.
- [26] A. Majewicz, J. J. Siegel, A. A. Stanley, and A. M. Okamura, "Design and evaluation of duty-cycling steering algorithms for robotically-driven steerable needles," in *Proc. IEEE Int. Conf. Robot. Autom. (ICRA)*, Hong Kong, May 2014, pp. 5883–5888, doi: 10.1109/ICRA.2014.6907725.
- [27] M. Mahvash and P. E. Dupont, "Fast needle insertion to minimize tissue deformation and damage," in *Proc. IEEE Int. Conf. Robot. Autom.*, Kobe, May 2009, pp. 3097–3102, doi: 10.1109/ROBOT.2009.5152617.
- [28] Y. Sun, "Study on robot-assisted system for percutaneous surgery based on 3D ultrasound images," Ph.D. dissertation, Dept. Mechatronics Eng., Harbin Inst. Technol., Harbin, China, 2011.
- [29] Y. Sun, D. Wu, Z. Du, and L. Sun, "Robot-assisted needle insertion strategies based on liver force model," *Robot.*, vol. 33, no. 1, pp. 66–70, Jan. 2011, doi: 10.3724/SP.J.1218.2011.00066.
- [30] Y. Zhang, W. Zhang, Y. Liang, and Y. Xu, "Research on mechanism and strategy of high accuracy puncture of prostate," *Chin. J. Sci. Instrum.*, vol. 38, no. 6, pp. 1405–1412, 2017, doi: 10.19650/j.cnki.cjsi.2017.06.012.
- [31] K. Reed, A. Majewicz, V. Kalleem, R. Alterovitz, K. Goldberg, N. Cowan, and A. Okamura, "Robot-assisted needle steering," *IEEE Robot. Autom. Mag.*, vol. 18, no. 4, pp. 35–46, Dec. 2011.
- [32] M. Li, G. Li, G. Berk, X. Duan, and I. Iulian, "Towards human-controlled, real-time shape sensing based flexible needle steering for MRI-guided percutaneous therapies," *Int. J. Med. Comput. Assist. Surg.*, vol. 13, no. 2, pp. 2–14, Jun. 2017.
- [33] Y. Fu, "Diagnosis value of shear wave elastography in benign and malignant prostatic diseases," M.S. thesis, Imag. Nucl. Med., North China Univ. Sci. Technol., TangShan, China, 2019.
- [34] X. Xu, "The value of shear wave elastography in diagnosis of benign prostatic hyperplasia," M.S. thesis, Clin., Imag. Nuclear Med., Lanzhou Univ., Lanzhou, China, 2016.
- [35] J. Ker, L. Wang, J. Rao, and T. Lim, "Deep learning applications in medical image analysis," *IEEE Access*, vol. 6, pp. 9375–9389, 2018.
- [36] R. J. S. Raj, S. J. Shobana, I. V. Pustokhina, D. A. Pustokhin, D. Gupta, and K. Shankar, "Optimal feature selection-based medical image classification using deep learning model in Internet of Medical Things," *IEEE Access*, vol. 8, pp. 58006–58017, 2020.
- [37] T. Brosch, L. Y. W. Tang, Y. Yoo, D. K. B. Li, A. Traboulsee, and R. Tam, "Deep 3D convolutional encoder networks with shortcuts for multiscale feature integration applied to multiple sclerosis lesion segmentation," *IEEE Trans. Med. Imag.*, vol. 35, no. 5, pp. 1229–1239, May 2016.
- [38] X. Qian, "Theoretical and experimental studies on dynamic characteristics of flexible spinning beams," Ph.D. dissertation, Dept. Mechatronics Eng., Harbin Inst. Technol., Harbin, China, 2011.
- [39] Y. Zhu and Y. Ren, "Free vibration analysis of horizontal spinning beams by using finite difference method," *J. Vib. Shock*, vol. 31, no. 14, pp. 43–46, Jul. 2012.
- [40] Y. Zhu and Y. Ren, "Analysis of bending vibration of rotating tapered beams based on finite difference method," *Noise Vib. Control*, vol. 34, no. 3, pp. 6–14, Jun. 2014, doi: 10.3969/j.issn.1006-1335.2014.03.002.
- [41] Y. Zennir, E. Mechhoud, A. Seboui, and R. Bendib, "Multi-controller approach with PSO-PI²D^μ controllers for a robotic wrist," in *Proc. 5th Int. Conf. Elect. Eng.-Boumerdes (ICEE-B)*, Boumerdes, Algeria, 2017, pp. 1–7, doi: 10.1109/ICEE-B.2017.8192224.
- [42] U. K. Acharya and S. Kumar, "Particle swarm optimization exponential constriction factor (PSO-ECF) based channel equalization," in *Proc. 6th Int. Conf. Comput. Sustain. Global Develop. (INDIACom)*, New Delhi, India, 2019, pp. 94–97.
- [43] W. Peng, Z. Yang, C. Liu, J. Xiu, and Z. Zhang, "An improved PSO algorithm for battery parameters identification optimization based on thevenin battery model," in *Proc. 5th IEEE Int. Conf. Cloud Comput. Intell. Syst. (CCIS)*, Nanjing, China, Nov. 2018, pp. 295–298, doi: 10.1109/CCIS.2018.8691341.
- [44] S. Bala and P. Pal, "An improved hybridization of tournament and genetic algorithm for solving various engineering design optimization problems," in *Proc. Michael Faraday IET Int. Summit*, Kolkata, India, 2015, pp. 638–640, doi: 10.1049/cp.2015.1707.
- [45] A. Wang, Y. Wen, W. L. Soong, and H. Li, "Application of a hybrid genetic algorithm for optimal design of interior permanent magnet synchronous machines," in *Proc. IEEE Conf. Electromagn. Field Comput. (CEFC)*, Miami, FL, USA, Nov. 2016, p. 1, doi: 10.1109/CEFC.2016.7816299.
- [46] S. Pravesjit and K. Kantawong, "An improvement of genetic algorithm for optimization problem," in *Proc. Int. Conf. Digit. Arts, Media Technol. (ICDAMT)*, Chiang Mai, Thailand, 2017, pp. 226–229, doi: 10.1109/ICDAMT.2017.7904966.
- [47] C. Fei, H. Liu, Z. Zhu, L. An, S. Li, and C. Lu, "Whole-process design and experimental validation of landing gear lower drag stay with global/local linked driven optimization strategy," *Chin. J. Aeronaut.*, Jul. 2020, pp. 1–7, doi: 10.1016/j.cja.2020.07.035.
- [48] C. Lu, Y.-W. Feng, C.-W. Fei, and S.-Q. Bu, "Improved decomposed-coordinated kriging modeling strategy for dynamic probabilistic analysis of multicomponent structures," *IEEE Trans. Rel.*, vol. 69, no. 2, pp. 440–457, Jun. 2020, doi: 10.1109/TR.2019.2954379.
- [49] J. Lü, Y. Yang, Q. Shang, Z. Li, J. Li, Z. Liu, and Y. Wang, "Performance optimization test on air-suction potato seed metering device with positive pressure airflow and zero-speed seeding," *Trans. Chin. Soc. Agricult. Eng.*, vol. 32, no. 20, pp. 40–48, Oct. 2016. [Online]. Available: <http://www.tcsae.org>, doi: 10.11975/j.issn.1002-6819.2016.20.005.
- [50] L. Qian, D. Xi, Y. Xiao, J. Wang, M. Zhang, H. Wang, and T. Zhang, "Parameters optimization and experiment of oriented alignment system for maize seed group based on electromagnetic vibration," *Trans. Chin. Soc. Agricult. Eng.*, vol. 33, no. 19, pp. 59–66, Oct. 2017. [Online]. Available: <http://www.tcsa.org>, doi: 10.11975/j.issn.1002-6819.2017.19.008.
- [51] S. Zhao, H. Tan, J. Wang, C. Yang, and Y. Yang, "Design and experiment of multifunctional integrated seeding opener," *Trans. Chin. Soc. Agricult. Eng.*, vol. 34, no. 11, pp. 58–67, Jun. 2018. [Online]. Available: <http://www.tcsae.org>, doi: 10.11975/j.issn.1002-6819.2018.11.008.
- [52] Z. Yuan, *Experiment Design and Analysis*. Beijing, China: Higher Education Press, 2000, pp. 360–372.
- [53] W. Wang, *Design and Analysis of Experiments*. Beijing, China: Higher Education Press, 2004, pp. 303–313.
- [54] C. Pang, *Optimal Design of Testing and Data Analysis*. NanJing, NJ, China: Southeast Univ. Press, 2018, pp. 154–165.
- [55] R. Girshick, J. Donahue, T. Darrell, and J. Malik, "Rich feature hierarchies for accurate object detection and semantic segmentation," in *Proc. IEEE Conf. Comput. Vis. Pattern Recognit.*, Jun. 2014, pp. 580–587.
- [56] P. Lyu, M. Liao, C. Yao, W. Wu, and X. Bai, "Mask textspotter: An end-to-end trainable neural network for spotting text with arbitrary shapes," in *Proc. Eur. Conf. Comput. Vis. (ECCV)*, 2018, pp. 67–83.
- [57] P. Rajpurkar, J. Irvin, K. Zhu, B. Yang, H. Mehta, T. Duan, D. Ding, A. Bagul, C. Langlotz, K. Shpanskaya, M. P. Lungren, and A. Y. Ng, "CheXNet: Radiologist-level pneumonia detection on chest X-Rays with deep learning," Dec. 2017, *arXiv:1711.05225*. [Online]. Available: <http://arxiv.org/abs/1711.05225>
- [58] B. Thananjeyan, A. Garg, S. Krishnan, C. Chen, L. Miller, and K. Goldberg, "Multilateral surgical pattern cutting in 2D orthotropic gauze with deep reinforcement learning policies for tensioning," in *Proc. IEEE Int. Conf. Robot. Autom. (ICRA)*, May 2017, pp. 2371–2378.
- [59] W. Xue, Q. Li, and Q. Xue, "Text detection and recognition for images of medical laboratory reports with a deep learning approach," *IEEE Access*, vol. 8, pp. 407–416, 2020.
- [60] S. Jiang, Z. Su, X. Wang, S. Liu, and Y. Yu, "Development of a new tissue-equivalent material applied to optimizing surgical accuracy," *Mater. Sci. Eng., C*, vol. 33, no. 7, pp. 3768–3774, Oct. 2013.
- [61] I. Bricault et al., "Light puncture robot for CT and MRI interventions," *IEEE Eng. Med. Biol. Mag.*, vol. 27, no. 3, pp. 42–50, May/Jun. 2008, doi: 10.1109/EMB.2007.910262.

- [62] M. Hadavand, M. D. Naish, and R. V. Patel, "A parallel remote center of motion mechanism for needle-based medical interventions," in *Proc. 5th IEEE RAS/EMBS Int. Conf. Biomed. Robot. Biomechatronics*, São Paulo, Brazil, Aug. 2014, pp. 1–6, doi: [10.1109/BIOROB.2014.6913742](https://doi.org/10.1109/BIOROB.2014.6913742).
- [63] A. Patriciu, D. Petrisor, M. Muntener, D. Mazilu, M. Schar, and D. Stoianovici, "Automatic brachytherapy seed placement under MRI guidance," *IEEE Trans. Biomed. Eng.*, vol. 54, no. 8, pp. 1499–1506, Aug. 2007, doi: [10.1109/TBME.2007.900816](https://doi.org/10.1109/TBME.2007.900816).
- [64] W. Yuan, B. Jiang, Y. Yang, and W. Wang, "Design of thoracoabdominal minimally invasive robot and kinematic analysis," *Mech. Sci. Technol. Aerosp. Eng.*, vol. 36, no. 11, pp. 1658–1665, Nov. 2017, doi: [10.13433/j.cnki.1003-8728.2017.1104](https://doi.org/10.13433/j.cnki.1003-8728.2017.1104).
- [65] N. Shi, H. Chen, X. Wang, Y. Chai, H. Wang, and S. Hou, "Design and experiment optimization of prevent bring back stubble mechanism of spring-tooth type cleaning device," *Trans. Chin. Soc. Agricult. Machinery*, vol. 50, no. 4, pp. 84–91, Apr. 2019, doi: [10.6041/j.issn.1000-1298.2019.04.010](https://doi.org/10.6041/j.issn.1000-1298.2019.04.010).
- [66] N. Shi, H. Chen, Z. Wei, Y. Chai, S. Hou, and X. Wang, "Design and test of forced-return device based on principle of brachistochrone," *Trans. Chin. Soc. Agricult. Machinery*, vol. 51, no. 2, pp. 37–44, Feb. 2020, doi: [10.6041/j.issn.1000-1298.2020.02.005](https://doi.org/10.6041/j.issn.1000-1298.2020.02.005).



YONGDE ZHANG was born in Jilin, China, in 1965. He received the B.S. degree in mechanical engineering and the M.S. degree from the Harbin Institute of Technology, Harbin, Heilongjiang, China, in 1988 and 1993, respectively, and the Ph.D. degree in mechanical engineering from the Harbin Institute of Technology, in 1999.

From 1999 to 2001, he worked as an Associate Researcher at the Automation Research Center, City University of Hong Kong. In 2004, he worked as a Researcher with the Computer-Assisted Interventional Medicine Laboratory, Nanyang Technological University, Singapore. From 2004 to 2006, he was a Visiting Scholar at the University of Rochester Medical Center. Since 2007, he has been a Professor and Doctoral Supervisor with the School of Mechanical Power Engineering and Robotics and its Engineering Research Center, Harbin University of Science and Technology. His current research interests include medical robots, education robots, and biomimetic robots.



BING LI was born in Heilongjiang, China, in 1988. He received the B.S. degree in mechanical engineering from the Heilongjiang Institute of Technology, Harbin, Heilongjiang, China, in 2012, and the M.S. degree from Northeast Agricultural University, Harbin. He is currently pursuing the Ph.D. degree in mechatronic engineering with the Harbin University of Science and Technology.

His current research interests include prostate particle implantation robot, electro-hydraulic servo control systems, and quadruped robot.



LIPENG YUAN was born in Inner Mongolia, China, in 1976. He received the B.S. degree in mechanical engineering, and the M.S. and Ph.D. degrees in mechanical engineering from the Harbin Institute of Technology, Harbin, Heilongjiang, China, in 1998, and 2000 and 2005, respectively.

He was a dual Postdoctoral Fellow with Cornell University, Ithaca, NY, USA, and the Harbin Institute of Technology. He once worked as a Lecturer at Cornell University as a Senior Engineer and Technical Consultant at e2eMaterials high-tech company, USA, and introduced into the United States as a high-tech special talent. He is currently the General Manager of the Nanjing Yuanling Digital Technology Co., Ltd., and an Associate Professor with the School of Mechanical and Electrical Engineering, Harbin Institute of Technology. His current researches include complex system statics and nonlinear dynamics analysis, hydraulic servo control theory, footed robots, entertainment and educational robots, and medical service robots.

• • •